Resource

Cell Stem Cell

CRISPR Interference Efficiently Induces Specific and Reversible Gene Silencing in Human iPSCs

Graphical Abstract

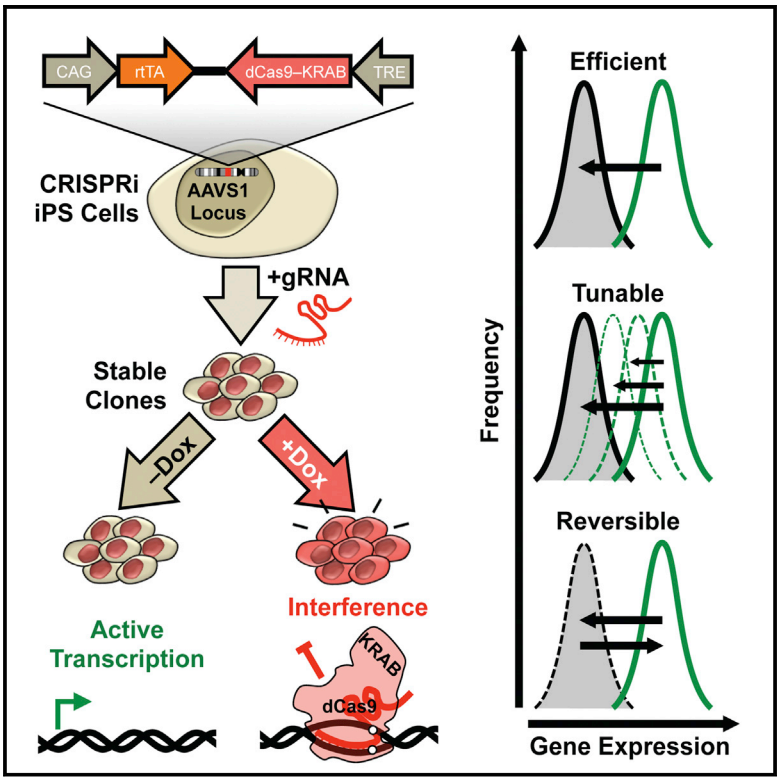

Highlights

- Inducible CRISPRi iPSCs provide a valuable resource for rapid gene knockdown
- CRISPRi knockdown is efficient, tunable, and reversible in iPSCs
- CRISPRi knockdown is highly specific
- CRISPRi enables disease modeling in iPSC-derived cardiomyocytes

Authors

Mohammad A. Mandegar, Nathaniel Huebsch, Ekaterina B. Frolov, ..., Lei S. Qi, Po-Lin So, Bruce R. Conklin

Correspondence

mo.mandegar@gladstone.ucsf.edu (M.A.M.), bconklin@gladstone.ucsf.edu (B.R.C.)

In Brief

In this article, Mandegar and colleagues utilize CRISPR interference for efficient gene knockdown in iPSCs and their differentiated cell derivatives. The CRISPRi tools and cell lines presented in this study are highly versatile and serve as a useful resource for the cell and stem cell biology communities.

Mandegar et al., 2016, Cell Stem Cell *18*, 541–553
April 7, 2016
http://dx.doi.org/10.1016/j.stem.2016.01.022

Cell Stem Cell
Resource

CRISPR Interference Efficiently Induces Specific and Reversible Gene Silencing in Human iPSCs

Mohammad A. Mandegar,[1,*] Nathaniel Huebsch,[1,2] Ekaterina B. Frolov,[1] Edward Shin,[1] Annie Truong,[1] Michael P. Olvera,[1] Amanda H. Chan,[1] Yuichiro Miyaoka,[1,12] Kristin Holmes,[1] C. Ian Spencer,[1] Luke M. Judge,[1,2] David E. Gordon,[3,4,5] Tilde V. Eskildsen,[6,7] Jacqueline E. Villalta,[3,4,8,9] Max A. Horlbeck,[3,4,8,9] Luke A. Gilbert,[3,4,8,9] Nevan J. Krogan,[3,4,5] Søren P. Sheikh,[6,7] Jonathan S. Weissman,[3,4,8,9] Lei S. Qi,[10] Po-Lin So,[1] and Bruce R. Conklin[1,3,4,11,*]
[1]Gladstone Institute of Cardiovascular Disease, San Francisco, CA 94158, USA
[2]Department of Pediatrics, University of California, San Francisco, San Francisco, CA 94158, USA
[3]Department of Cellular and Molecular Pharmacology, University of California, San Francisco, San Francisco, CA 94158, USA
[4]California Institute for Quantitative Biosciences, QB3, University of California, San Francisco, San Francisco, CA 94158, USA
[5]Gladstone Institute of Virology and Immunology, San Francisco, CA 94158, USA
[6]Department of Cardiovascular and Renal Research, University of Southern Denmark, 5000 Odense C, Denmark
[7]Department of Clinical Biochemistry and Pharmacology, Odense University Hospital, 5000 Odense C, Denmark
[8]Howard Hughes Medical Institute, University of California, San Francisco, San Francisco, CA 94158, USA
[9]Center for RNA Systems Biology, University of California, San Francisco, San Francisco, CA 94158, USA
[10]Department of Bioengineering, Stanford University, Stanford, CA 94305, USA
[11]Department of Medicine and Cellular and Molecular Pharmacology, University of California, San Francisco, San Francisco, CA 94158, USA
[12]Present address: Regenerative Medicine Project, Tokyo Metropolitan Institute of Medical Science, Tokyo, 156-8506, Japan
*Correspondence: mo.mandegar@gladstone.ucsf.edu (M.A.M.), bconklin@gladstone.ucsf.edu (B.R.C.)
http://dx.doi.org/10.1016/j.stem.2016.01.022

SUMMARY

Developing technologies for efficient and scalable disruption of gene expression will provide powerful tools for studying gene function, developmental pathways, and disease mechanisms. Here, we develop clustered regularly interspaced short palindromic repeat interference (CRISPRi) to repress gene expression in human induced pluripotent stem cells (iPSCs). CRISPRi, in which a doxycycline-inducible deactivated Cas9 is fused to a KRAB repression domain, can specifically and reversibly inhibit gene expression in iPSCs and iPSC-derived cardiac progenitors, cardiomyocytes, and T lymphocytes. This gene repression system is tunable and has the potential to silence single alleles. Compared with CRISPR nuclease (CRISPRn), CRISPRi gene repression is more efficient and homogenous across cell populations. The CRISPRi system in iPSCs provides a powerful platform to perform genome-scale screens in a wide range of iPSC-derived cell types, dissect developmental pathways, and model disease.

INTRODUCTION

To understand the biological roles of genes in development and disease, we must decipher the relationships between genotype and phenotype. Until recently, RNAi has been the most commonly used loss-of-function tool to study human biology (Boettcher and McManus, 2015). However, RNAi suffers from off-target effects and incomplete silencing of the desired gene (Jackson et al., 2003; Kim et al., 2013b; Krueger et al., 2007). Alternatively, programmable nucleases, such as zinc-finger nucleases (ZFNs) and transcription activator-like effector nucleases (TALENs), allow more precise gene editing in model organisms, particularly in mammalian and human systems (Gaj et al., 2013; Kim and Kim, 2014). While ZFNs and TALENs are efficient tools for targeting single alleles, they cannot be easily used for library-scale loss-of-function studies.

In 2012, clustered regularly interspaced short palindromic repeat (CRISPR) technology emerged as a new tool for gene editing. This technology is a microbial adaptive-immune system that uses RNA-guided nucleases to recognize and cleave foreign genetic elements (Doudna and Charpentier, 2014; Wiedenheft et al., 2012). The recently engineered CRISPR/Cas9 system consists of two components: a single-chimeric guide RNA (gRNA) that provides target specificity and a CRISPR-associated protein (Cas9) that acts as a helicase and a nuclease to unwind and cut the target DNA (Cong et al., 2013; Mali et al., 2013). In this system, the only restriction for targeting a specific locus is the protospacer adjacent motif (PAM) sequence ("NGG" in the case of *Sp*Cas9) (Doudna and Charpentier, 2014).

CRISPR nuclease (CRISPRn) has been used for genome-scale screens to identify essential genes for cell viability in cancer and embryonic stem cells (Shalem et al., 2014) and human leukemic cell lines (Wang et al., 2014, 2015). However, CRISPRn may not be the most robust system for loss-of-function studies, because it is limited by the number of cells within a population that do not produce knockout phenotypes (González et al., 2014). In addition, partial loss- or gain-of-function phenotypes can be generated by Cas9-induced in-frame insertion/deletions (INDELs) and hypomorphic alleles (Shi et al., 2015), which can obscure the readout.

The nuclease deactivated version of Cas9 (dCas9) blocks transcription in prokaryotic and eukaryotic cells (known as CRISPR interference; CRISPRi) (Qi et al., 2013). More recently, dCas9 was fused to the Krüppel-associated box (KRAB) repression domain to generate dCas9-KRAB, producing a

more efficient transcriptional interference (Gilbert et al., 2013, 2014; Kearns et al., 2014). To further this effort, we aimed to use CRISPRi technology to efficiently repress genes to study early differentiation and model disease with human induced pluripotent stem cells (iPSCs) (Takahashi et al., 2007).

iPSCs are well suited to study early embryonic development and disease since they can produce different functional cell types in vitro (Sterneckert et al., 2014). Early embryonic development consists of a series of accurately timed events that affect gene activation and repression (Bolouri and Davidson, 2003). Therefore, precisely regulating the timing and dosage of transcription factors critically affects embryonic development (McFadden et al., 2005; Takeuchi et al., 2011), and dysregulation in the timing and dosage of transcripts can lead to disease development (Theodoris et al., 2015). In this study, we compared inducible CRISPR systems for gene knockout (using Cas9) or knockdown (using dCas9-KRAB) to enable temporal control of loss-of-function phenotypes in iPSCs and differentiated cell types.

RESULTS

Generation of CRISPRi and CRISPRn iPSC Lines

For loss-of-function studies, we independently derived multiple stable CRISPRi and CRISPRn human iPSC clones in two genetic backgrounds: wild-type B (WTB) and wild-type C (WTC) (Miyaoka et al., 2014). In separate targeting events, the CRISPRi and CRISPRn constructs (see Supplemental Experimental Procedures) were integrated into the AAVS1 locus of WTB and WTC iPSCs using a TALEN-assisted gene-trap approach (Figures 1A, 1B, and S1). Transgenes integrated at the AAVS1 locus remain transcriptionally active in both iPSCs and differentiated cell types (Hockemeyer et al., 2011; Lombardo et al., 2011). We generated several different versions of the CRISPRi system that are either inducible or constitutive; the inducible CRISPRi (Gen1 and Gen2) clones express dCas9-KRAB (KRAB domain fused at the N terminus) from the inducible TetO promoter, while the constitutive CRISPRi clones (Gen3) express dCas9-KRAB under the constitutively active CAG promoter. The CRISPRn (Gen1) clones express Cas9 under the inducible TetO promoter (Figure S1).

The average efficiency of forming stable clones was ~350 colonies per million iPSCs transfected with AAVS1 TALENs and donor plasmid (data not shown). From each condition, multiple independent colonies were isolated and expanded. A subset of the stable colonies from each targeting vector was screened using junction PCR. Two putative colonies from each targeting event were further characterized by stably introducing an *OCT4*-specific gRNA and performing knockdown or knockout assays with immunofluorescence and western blot analysis. All putative CRISPRi clones containing an *OCT4*-specific gRNA showed efficient knockdown (>95%) of OCT4 in bulk populations, while a significant fraction of the CRISPRn cells remained OCT4 positive (~30%–40%) in bulk populations containing *OCT4*-specific gRNA (Figure S1). One clone each from CRISPRi and CRISPRn (Gen1 lines in the WTC genetic background) were subsequently used as lead clones for further studies.

To enable non-invasive and high-throughput phenotypic analysis in iPSC-derived cardiomyocytes (iPS-CMs), we performed a second targeting event that introduced the green fluorescent calcium-modulated protein 6 fast type (GCaMP) calcium sensor (Chen et al., 2013) into the other AAVS1 locus of the CRISPRi cell line. The GCaMP transgene is driven off the strong, constitutive CAG promoter (Figure S1). We found that CRISPRi iPSCs could differentiate into iPS-CMs, so that we could measure calcium transients based on the GCaMP-fluorescent intensity (Movie S1) (Huebsch et al., 2015). Lead CRISPRi and CRISPRn iPSCs were karyotypically normal (Figures S2A and S2B) and expressed pluripotency markers, as expected (Figures S2C and S2D).

RNA-sequencing (RNA-seq) analysis indicated that expression of dCas9-KRAB or Cas9 was undetectable in the absence of doxycycline, and addition of doxycycline without any gRNA resulted in robust selective induction of dCas9-KRAB or Cas9, while the rest of the transcriptome remained virtually unchanged (Figures S2E and S2F). Furthermore, the RNA-seq data suggest that the addition of the KRAB domain has no detectable off-target effects when compared to expression of Cas9 alone. Remarkably the one gene that appeared to be upregulated upon doxycycline induction (without gRNA) was the same gene (Vimentin; *VIM*) for both CRISPRi and CRISPRn cells (Figures S2E and S2F). Since the same gene is upregulated for CRISPRi and CRISPRn cells, we suspect it may represent an off-target activity of the doxycycline-induced transactivator. Importantly, our experiments suggest that the expression of dCas9-KRAB alone has no additional effects on gene expression.

We also expressed dCas9-KRAB and Cas9 by continuously culturing CRISPRi and CRISPRn lines with doxycycline for 3 weeks (four passages). With this long-term treatment, we observed no cytotoxicity, decrease in proliferation, or change in morphology in these cells (Figures S2G and S2H). Using a droplet digital PCR (ddPCR)-based copy-number assay, we measured the number of integration events (Figure S2I). We further validated on-target integration sites on the lead CRISPRi and CRISPRn clones with junction PCR (Figure S2J) and verified their sequences (data not shown).

To further ensure there was no leaky expression of the single doxycycline-inducible vector, we measured the protein levels of dCas9-KRAB and Cas9 in iPSCs. With immunostaining, flow cytometry and western blots did not detect dCas9-KRAB or Cas9 protein without doxycycline in either CRISPRi or CRISPRn iPSCs, indicating that the TetO promoter has high fidelity in the AAVS1 locus. After doxycycline treatment, all cells in the CRISPRi and CRISPRn lines expressed dCas9-KRAB or Cas9 within 48 hr, respectively (Figures 1C–1H). dCas9-KRAB and Cas9 were expressed at similar levels after induction, and both proteins rapidly degraded after removing doxycycline (Figures 1F, 1H, and S2K). These data showed that dCas9-KRAB and Cas9 expression could be tightly regulated with the TetO promoter, which would support studies that rely on precisely timing gene knockdown or knockout.

Comparison of Loss of Function between CRISPRi and CRISPRn

To compare CRISPRi and CRISPRn for loss-of-function studies, we designed a gRNA that targets the first exon of *NANOG*, a transcription factor necessary for maintaining the pluripotency network. We selected *NANOG* as our first target gene because its deficiency is sufficient to give an immediate readout, as

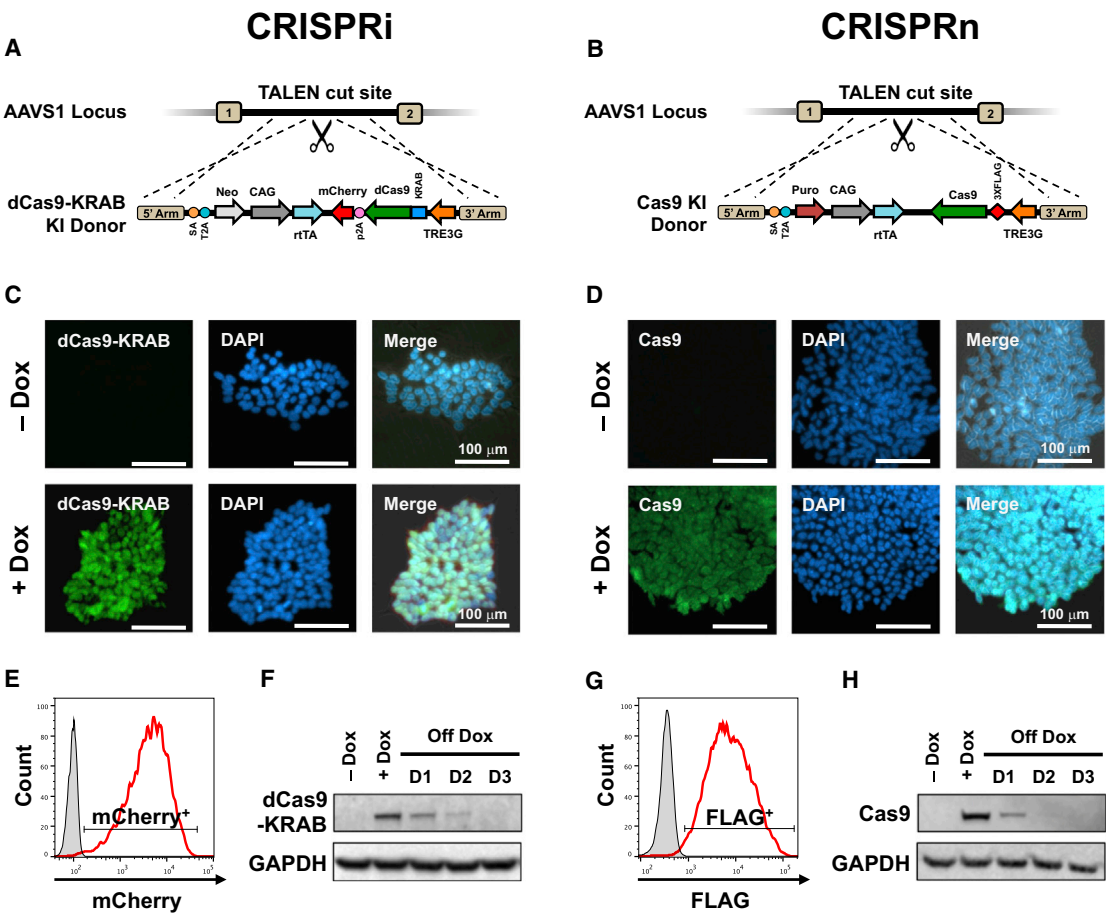

Figure 1. Generation and Characterization of Inducible CRISPRi and CRISPRn iPSCs

(A and B) Schematic overview of the strategy for TALEN-mediated targeting to the AAVS1 locus to generate the CRISPRi and CRISPRn iPSC lines. The doxycycline-controlled reverse transcriptional activator (rtTA) is driven by a strong constitutive promoter (CAG). The third-generation doxycycline-response element (TRE3G) drives transcription of either Cas9 (CRISPRn) or dCas9-KRAB-P2A-mCherry (CRISPRi) and is oriented in the opposite direction of the transactivator to ensure no leaky expression without doxycycline treatment.

(C and D) Immunostaining of CRISPRi and CRISPRn colonies before and after 48 hr of doxycycline treatment with an antibody against Cas9 (green). Nuclei are stained with DAPI (blue). All nuclei showed expression of dCas9-KRAB or Cas9 after adding doxycycline.

(E and G) Flow cytometry analysis of CRISPRi and CRISPRn iPSC lines before and after 48 hr of doxycycline treatment. Doxycycline treatment of CRISPRi and CRISPRn produced expression of mCherry and FLAG in all cells, respectively. The doxycycline-untreated sample is plotted in gray.

(F and H) CRISPRi and CRISPRn iPSC lines were treated with doxycycline (2 μM) for 24 hr, which was then removed to measure the protein half-life of dCas9-KRAB and Cas9. Total protein was extracted from samples and analyzed by western blot with antibodies against Cas9 and GAPDH as a loading control. Both the CRISPRi and CRISPRn clones express dCas9-KRAB and Cas9 at similar levels after doxycycline treatment, and the half-life of both proteins was ~12 hr in iPSCs. Scale bars, 100 μm.

indicated by a clear loss of pluripotent cell morphology (Hayashi et al., 2015). In general, Cas9 can disrupt gene function at any given exon (Doench et al., 2014), while dCas9-KRAB knocks down gene expression only when gRNAs are targeted to the transcription start site (TSS) (Gilbert et al., 2014). Hence, for this comparative study, we used the same gRNA sequence for both CRISPRi and CRISPRn. Here, we introduced a gRNA targeting 358 bp downstream of the *NANOG* TSS (142 bp into exon 1 of *NANOG*) into the CRISPRi and CRISPRn clones and selected subclones (as described in Experimental Procedures). We then treated multiple independent subclones of CRISPRi and CRISPRn iPSCs containing the *NANOG* gRNA-expression vector (as indicated by mKate2 expression) with doxycycline (Figure 2).

With CRISPRi, we found that NANOG expression was completely lost (>99%) in multiple independent iPSC subclones after doxycycline treatment (Figures 2A, 2C, 2E, S3A, and S3C). However, with CRISPRn, only 60%–70% of the cells lost NANOG expression in multiple independent subclones post-doxycycline induction (Figures 2B, 2D, 2G, S3B, and S3D). Next, we extracted genomic DNA from *NANOG* gRNA-containing CRISPRi and CRISPRn iPSCs and performed sequence analysis. As expected, we found that CRISPRi iPSCs did not harbor any mutations in the *NANOG* locus pre- or post-doxycycline treatment (Figure 2F). However, with CRISPRn, after 12–17 days of continuous doxycycline treatment, among the mutated alleles, 30%–50% of the sequences contained in-frame INDELs at the cut site (a total of 77 sequenced clones) (Figure 2H).

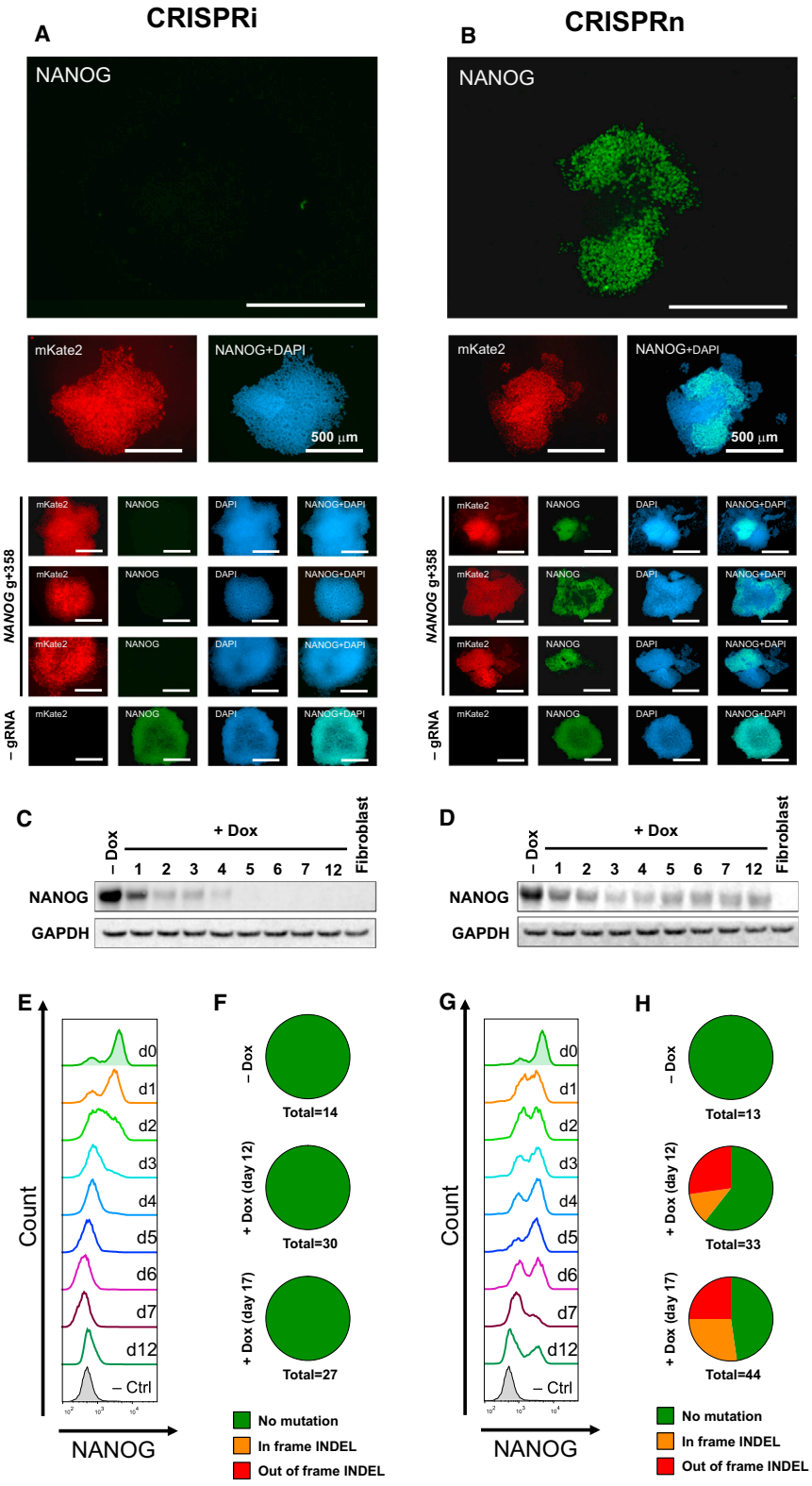

Figure 2. Comparison of the Efficiency of CRISPRi Knockdown and CRISPRn Knockout

(A and B) Immunostaining of representative (A) CRISPRi and (B) CRISPRn stable clones, each containing the same gRNA targeting the first exon of *NANOG* (*NANOG* g+358). After 7 days of doxycycline treatment, *NANOG* expression (green) was completely lost in all CRISPRi clones but showed a variegated pattern of knockout in multiple independent CRISPRn clones. The mKate2 signal indicates the presence of the gRNA-expression vector in all cells within the clone. Nuclei are counterstained with DAPI.

(C, D, E, and G) Western blot and flow cytometry analyses of (C and E) CRISPRi and (D and G) CRISPRn stable clones that contain the same gRNA against the first exon of *NANOG*. With CRISPRi, *NANOG* expression was uniformly decreased during doxycycline treatment and did not increase thereafter; however, with CRISPRn, the percentage of NANOG-positive cells fluctuated during doxycycline treatment. Even after 12 days of continuous doxycycline treatment, ~30% of the population stained positive for NANOG.

(F and H) Genomic DNA was extracted from (F) CRISPRi and (H) CRISPRn stable lines containing a gRNA against *NANOG* before and after continuous doxycycline treatment for up to 17 days and subjected to sequencing. Red, out-of-frame INDELs; orange, in-frame INDELs; green, non-mutated alleles. Even after 12–17 days of continuous doxycycline treatment, 50%–70% of sequenced alleles from CRISPRn contained no mutation, and 30%–50% of mutated alleles were in-frame INDELs. No mutations were observed in either CRISPRi or CRISPRn without doxycycline, and the CRISPRi clones did not contain any mutations after doxycycline treatment. The total number of sequenced colonies is listed below each pie graph.

Scale bars, 500 μm.

To further compare CRISPRi with CRISPRn, we targeted another pluripotency transcription factor, *OCT4*, with two independent gRNAs. Similar to our findings with *NANOG*, *OCT4* was completely knocked down in independent CRISPRi clones expressing the gRNA vector after doxycycline treatment (Figure S3E). In contrast, the attempted knockout of OCT4 with CRISPRn again yielded incomplete effects (Figure S3F). These findings were also replicated in a completely different iPSC line (WTB genetic background; CRISPRi Gen1B and CRISPRn Gen1B) (Figures S1D and S1F). We analyzed the genomic DNA of CRISPRn cells after 14 days of continuous doxycycline treatment and found 30%–40% of the mutated alleles had in-frame INDELs (a total of 91 sequenced clones) (Figure S3G). These results suggested that, in the context of targeting pluripotency factors, CRISPRi more rapidly generates loss-of-function phenotypes in bulk populations than CRISPRn. CRISPRi caused a complete

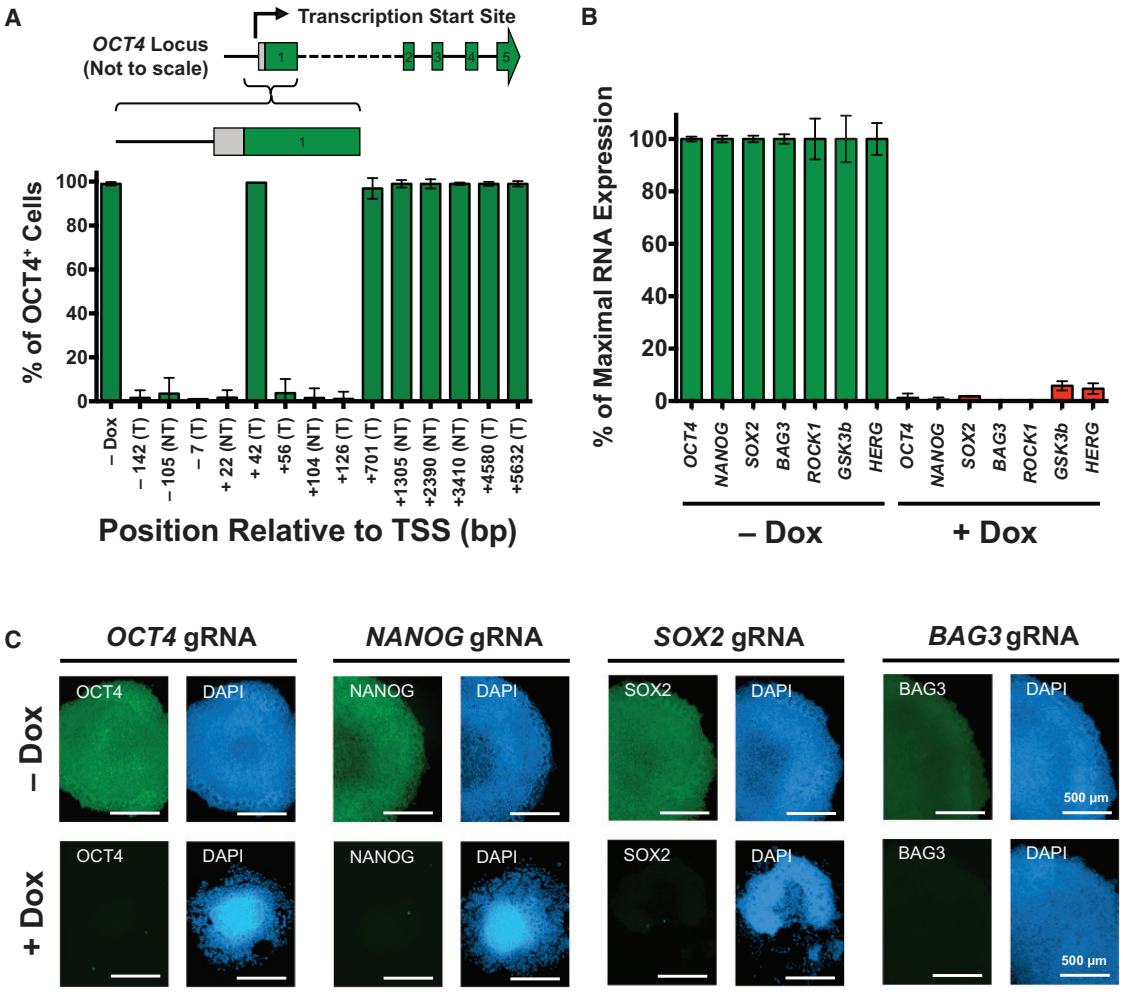

Figure 3. CRISPRi Knockdown Is Efficient in iPSCs

(A) Efficiency of gRNA knockdown based on proximity to the transcription start site (TSS). The binding location of each gRNA is indicated relative to the TSS of the *OCT4* locus and whether it targets the template (T) or non-template (NT) strand. Only gRNAs targeting near the TSS (approximately ±150 bp) effectively knocked down *OCT4*.

(B) TaqMan qPCR analysis of stable iPSCs containing gRNA against the gene of interest showed greater than 90% knockdown efficiency after 7 days of doxycycline induction in different endogenous genetic loci.

(C) Immunostaining of stable clones containing a single gRNA against the gene of interest (*OCT4, SOX2*, *NANOG,* and *BAG3*). After 7 days of doxycycline treatment, there was a complete knockdown of the protein of interest (green). As expected, DAPI staining revealed that knocking down *OCT4*, *NANOG* and *SOX2* resulted in loss of pluripotency and clear morphological changes. Also, knocking down *BAG3* did not cause a loss of pluripotent morphology, as indicated by the distinct and round colony edges.

Error bar represents SD.

loss of transcript expression and rapid cell differentiation when targeting *NANOG* and *OCT4* within 5–7 days of knockdown initiation. With CRISPRn, even after ~2 weeks of doxycycline treatment, a significant fraction (30%–40%) of the cells remained NANOG and OCT4 positive and maintained their pluripotency. Therefore, we focused on using CRISPRi as a loss-of-function tool in subsequent experiments.

CRISPRi Is Most Effective near the TSS

To further test the efficacy of gRNAs in CRISPRi, we designed multiple gRNAs that target near the TSS of OCT4. With flow cytometry assays for OCT4 staining (Figure 3A), we found that most gRNAs targeting near the TSS (approximately −150 bp to +150 bp around the TSS in this study) were highly effective at gene knockdown, but gRNAs targeting significantly (>700 bp) downstream of the TSS were not. This result agrees with previous data (Gilbert et al., 2014) and suggests that CRISPRi primarily blocks transcription at initiation, which reduces the likelihood of off-target effects from transcript interference elsewhere in the genome. Following these design criteria, for subsequent gene targets, we designed gRNAs to target near the TSS.

CRISPRi Efficiently Knocks Down a Broad Range of Genetic Loci

To test the efficiency of CRISPRi across a broad range of genetic loci in both iPSCs and differentiating/differentiated cell types, we

designed gRNAs against a total of nine genomic loci. The loci included core pluripotency transcription factors (*OCT4*, *NANOG*, and *SOX2*), kinases (*ROCK1* and *GSK3-β*), a cardiac mesoderm-transcription factor (*MESP1*), and cardiac disease-associated genes (*BAG3*, *MYBPC3*, and *HERG*). Except for *MESP1* (expressed only transiently in cardiac mesoderm cells) and *MYBPC3* (expressed only in cardiomyocytes), all other genes are expressed in iPSCs at different levels. We generated populations of CRISPRi iPSCs containing stably integrated gRNA-expression constructs. We then cultured these stable polyclones or clonal populations either with or without doxycycline for at least 7 days.

Three to five gRNAs were designed to target near the TSS of each gene and initially were tested individually in polyclonal populations. Approximately half of the tested gRNAs were active in polyclonal populations with a silencing activity of over 70% (Figure S4A). We did not observe a difference in the knockdown efficiency between gRNAs targeting either the template or non-template strands (Figures 3A, S4A, and S4B). The most active gRNA-containing polyclonal line was further passaged and subcloned for more detailed knockdown analysis. Using the most active gRNA, we achieved 90%–99% knockdown of the gene of interest in a selected population of iPSCs after doxycycline treatment (Figure 3B). As expected, when we subcloned polyclonal populations via single-cell cloning, we observed a higher percentage of transcriptional knockdown. With immunofluorescence analysis we found that iPSC clones expressing gRNAs against *OCT4*, *NANOG*, *SOX2*, and *BAG3* showed complete loss of target protein expression 7 days after doxycycline induction. In cells expressing gRNAs against the core pluripotency transcription factors *OCT4*, *NANOG*, and *SOX2*, we observed clear morphological changes and a loss of pluripotency after doxycycline induction; however, loss of a non-pluripotency gene (*BAG3*) did not affect pluripotent morphology (Figure 3C).

Using the Gen1 CRISPRi knockin vector, we targeted non-iPSCs with a different genetic background to determine how broadly this technology can be applied to other cell types. A T-lymphocyte (CEM) CRISPRi line was generated, as described in Experimental Procedures. Similar to the iPSC experiments, gRNAs were introduced to the stable CEM CRISPRi cell line, and cells cultured in either the presence or absence of doxycycline for 10 days. Three gRNAs were tested to knock down *CD4* in CEM-CRISPRi cells, and all showed greater than 70% knockdown efficiency in polyclonal populations (Figure S4B). The most active gRNA-containing polyclone was subcloned, and three independent clonal lines were isolated and assayed for knockdown, where greater than 95% knockdown efficiency was observed (Figure S4C). These results clearly demonstrate the doxycycline-inducible CRISPRi vector system is highly versatile and transportable to other cell lines and shows high efficiency of knockdown across a range of cell types and genetic loci.

CRISPRi Knockdown Is Reversible and Tunable and Can Be Allele Specific

GCaMP is a calcium-sensitive modified GFP and, thus, can be used as a fluorescent reporter under steady-state levels of cytoplasmic Ca^{2+} (Apáti et al., 2013). Using GCaMP (driven off the strong constitutive promoter, CAG), we monitored the green-fluorescence signal in iPSCs to determine if we could knock down GCaMP and then reverse its expression by removing doxycycline from the culture. We found that adding doxycycline for 7 days knocked down GCaMP expression by 98%, which was completely restored after removing doxycycline for 14 days (Figure 4A). Similarly, we targeted the *BAG3* endogenous locus and achieved efficient transcript knockdown post-doxycycline treatment. *BAG3* expression was fully restored after doxycycline withdrawal (Figure 4B). These findings indicate that CRISPRi knockdown is fully reversible in iPSCs.

To determine if we could achieve variable levels of knockdown with different gRNA sequences, we tested two additional gRNAs targeting GCaMP (g+24 and g+91) (Figure 4C). These gRNAs knocked down GCaMP expression by only ~30% and ~50%, as measured by flow cytometry (Figures 4D and 4E). Therefore, by changing the location of the gRNA-binding site, we can tune the level of knockdown when trying to mimic haploinsufficiency or reduced protein levels (rather than complete loss of function). In addition, we tested whether the knockdown level is tunable by titrating the doxycycline concentration. Careful titration of the doxycycline concentration enabled homogenous modulation of GCaMP expression (Figure S5).

We next sought to further test the tunability of knockdown with CRISPRi. We determined if we could use single-nucleotide polymorphisms (SNPs) to specifically target one allele for knockdown to achieve a heterozygous-like state. In our CRISPRi iPSCs, there is a SNP near the TSS of *OCT4*. Thus, we designed a gRNA in which the heterozygous SNP is located in the PAM sequence (AGG versus AGA). Because an "NGG" sequence is required for dCas9 to target DNA, we could selectively target only one *OCT4* allele (Figure 4F). After doxycycline induction, we found that the iPSC population carrying the SNP-specific *OCT4* gRNA (*OCT4* g−4) remained OCT4 positive (~97%) by flow cytometry analysis. However, the median intensity of OCT4 staining was reduced by ~40% after 7 days of doxycycline treatment, implying that OCT4 expression was homogeneously reduced in all cells and not just a fraction of them (Figures 4G and 4H). We confirmed this finding with immunocytochemistry and TaqMan qPCR (data not shown).

CRISPRi Knockdown Is Highly Specific

To assess the specificity of CRISPRi targeting, we designed a gRNA that targets the GCaMP transgene, since its silencing should have few downstream transcriptional and cellular consequences. Indeed, expression of the GCaMP transcript was over 30-fold lower in the doxycycline-treated condition, while few other endogenous transcripts changed expression level with the exception of *VIM* as previously discussed (Figure 5A).

CRISPRi to Promote iPSC Differentiation

To show that our system can release iPSCs from their pluripotent state to promote differentiation, we tested the efficiency of CRISPRi in knocking down core pluripotency transcription factors (*OCT4*, *SOX2*, and *NANOG*) without adding small molecules or cytokines to the mTeSR media. We targeted gRNA against these genes and performed a time-course analysis of a selected number of transcripts by TaqMan qPCR (Figure 5B). We found that knocking down these target transcripts caused cell differentiation, as indicated by morphological changes and transient expression of the lineage-specific transcript *T* (mesoderm marker), and expression of *PAX6* (neuronal progenitor marker). After 3 days

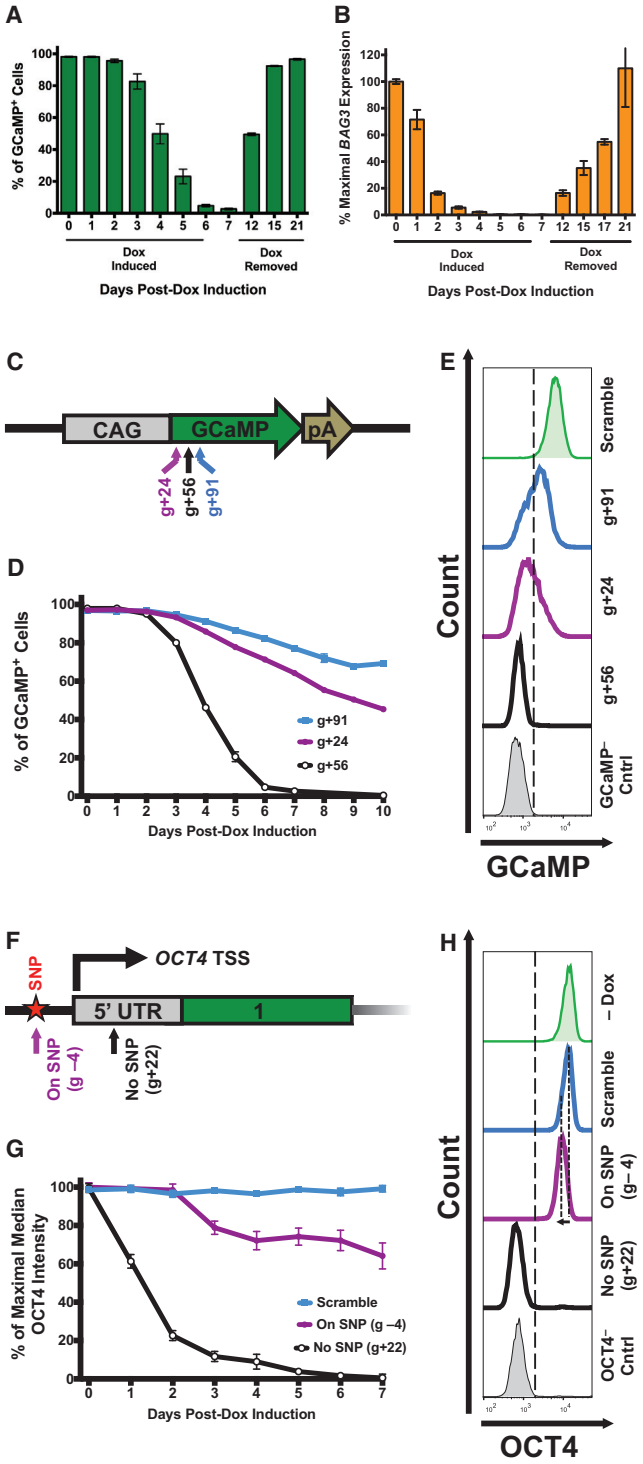

Figure 4. CRISPRi Knockdown Is Reversible and Tunable

A CRISPRi clone containing gRNA against the GCaMP transgene (GCaMP g+56) and endogenous *BAG3* locus were used to test the knockdown efficiency and reversibility of the CRISPRi system in iPSCs.

(A) Flow cytometry analysis of GCaMP expression showed that after 7 days of doxycycline induction, GCaMP was knocked down by ~99% and was completely restored after doxycycline withdrawal for 14 days.

(B) Using TaqMan qPCR, *BAG3* transcript levels were knocked down to nearly undetectable levels, and expression was restored after doxycycline withdrawal.

(C) Schematic diagram of the GCaMP-expression vector in which the GCaMP open reading frame (ORF) is driven off the CAG promoter. The locations of three gRNAs (g+24, g+56, and g+91) are schematically highlighted on the GCaMP ORF. The coordinates of GCaMP gRNA are based on the translation start site. pA, poly A signal.

(D) Three stable CRISPRi colonies, each containing a different gRNA against GCaMP, were selected using blasticidin and cultured with doxycycline for 10 days. The percentage of GCaMP-positive cells for each gRNA-containing clone was plotted as a function of time based on flow cytometry analysis. Variable levels of GCaMP knockdown (~30%, ~50%, and ~99%) were achieved with different gRNA sequences. n = 1–3 technical replicates for each time point.

(E) Flow cytometry plots of GCaMP fluorescence of stable CRISPRi clones on day 10 of doxycycline treatment. Using different gRNAs that target near the same region, variable levels of knockdown can be achieved. A scramble gRNA-containing CRISPRi and a GCaMP-negative iPSC population are displayed as controls.

(F) Partial schematic diagram of the *OCT4* locus marked with the location of the TSS and two gRNA-binding locations. Asterisk, an SNP; green box, exon 1; gray box, 5′ UTR.

(G) Three stable CRISPRi colonies, two with different gRNAs against *OCT4* and one with a scrambled control, were selected with blasticidin. Stable clones that contain either a scramble gRNA, a gRNA that targets a PAM sequence containing a SNP (*OCT4* g–4), or a gRNA that does not target a SNP (*OCT4* g+22) were treated with doxycycline. The percentage of the maximal median intensity of OCT4 staining for each gRNA-containing clone is plotted as a function of time by flow cytometry analysis. Complete loss of *OCT4* expression (>98% knockdown) was observed after 7 days of doxycycline induction only when both alleles were targeted using *OCT4* g+22. While using *OCT4* g–4, which targets only one *OCT4* allele (due to SNP in the PAM sequence), a gradual loss of OCT4 staining intensity is observed over time (down by ~40% by day 7). Error bars represent SD; n = 1–3 technical replicates for each time point.

(H) Flow cytometry plots of OCT4 staining on day 7 of doxycycline treatment. Dashed lines highlight the loss of OCT4-staining intensity (~40%) when using *OCT4* g–4 compared to the scramble control. By targeting only one allele of *OCT4*, the OCT4-staining intensity homogeneously shifts (while remaining OCT4-positive), indicating that each cell experiences approximately the same level of knockdown. Note that the x axis is a log-scale of OCT4 intensity. Differentiated iPSC-derived fibroblasts (OCT4$^-$ Cntrl) and a non-doxycycline-treated (–Dox) sample are displayed as controls.

Error bars represent SD.

of doxycycline treatment, over 80% of the target transcript was depleted, indicating that CRISPRi can precisely and temporally control efficient knockdown of the transcript of interest.

CRISPRi Knockdown in Cardiac Mesoderm and iPS-CMs

To determine if loss-of-function approaches using CRISPRi can be applied in differentiated cell types, we targeted the cardiac mesoderm-specific transcription factor (*MESP1*) and two known cardiac-related disease-causing genes (*MYBPC3* and *HERG*). We established stable polyclonal lines of iPSCs containing gRNA against these three genes and differentiated them into cardiac mesoderm or iPS-CMs as described in Experimental Procedures (Figures S6A and S6B). Using a gRNA against these genes, *MESP1* was knocked down by ~90% in cardiac progenitor cells, and *MYBPC3* and *HERG* by ~90% and 60%, respectively, in lactate-purified iPS-CMs (Figure 6A). With western blots and immunocytochemistry, we observed ~90% MYBPC3 protein knockdown on day-35 lactate-purified iPS-CMs (Figures 6B and 6C).

Using flow cytometry, we analyzed the doxycycline response of CRISPRi cells based on mCherry expression (as a surrogate

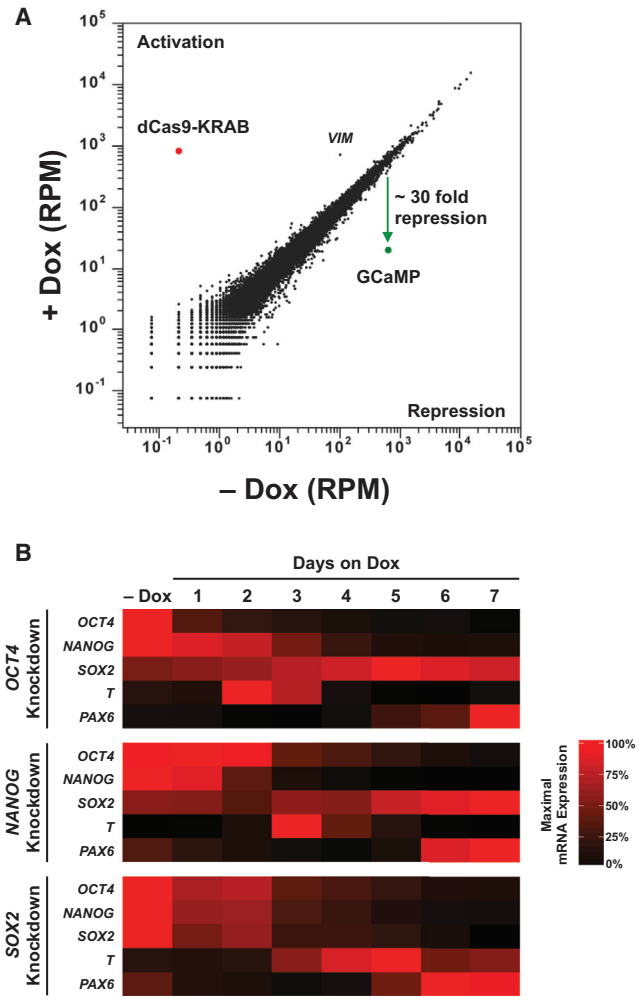

Figure 5. RNA-Seq and TaqMan qPCR Analysis

(A) RNA-sequencing RPMs (reads per million) are plotted for CRISPRi cells stably expressing a gRNA targeting the GCaMP transgene (GCaMP g+56) cultured in the absence or presence of doxycycline. CRISPRi knockdown is specific to the GCaMP transcript, and few off-target transcriptional changes were observed. Data represent two independent biological replicates.

(B) Heatmap of TaqMan qPCR of stable clones containing a single gRNA against the gene of interest (*OCT4*, *NANOG*, and *SOX2*) as a function of days after doxycycline treatment. Analysis shows that by day 3, over 80% of the target transcript is depleted. Three housekeeping genes (*18S*, *GAPDH*, and *UBC*) were used to measure relative transcript levels. Each data point is an average of two to four technical replicates. TaqMan probes are listed in Supplemental Experimental Procedures.

for dCas9-KRAB expression; Figure S5A). There was no silencing of the TetO promoter in low-passage and high-passage iPSCs, suggesting that long-term culturing (>3 months) does not cause silencing. However, cardiac progenitors (day 5) and iPS-CMs (day 15) lose ~20% and 50%–80% of the doxycycline response, respectively. Prolonging the duration of doxycycline treatment (from 2 to 7 days) and splitting the cells improved doxycycline response (as measured by mCherry expression) in iPS-CMs (Figure S6C). For this reason, we initiated all of our knockdowns on day 5 post-differentiation to obtain the maximum amount of target gene silencing. It is worth noting that with CRISPRi, only minute amounts of the dCas9-KRAB protein are necessary to induce a knockdown. Hence, knockdown might occur even in cells that do not show detectable mCherry expression (Figure S5).

The knockdown of the *HERG* potassium channel in iPSCs was highly efficient (>95%), while in iPS-CMs it was only 60% effective. We hypothesize that the reduction in the efficiency of *HERG* knockdown is partially due to activation of other *HERG* isoforms in iPS-CMs. We further investigated whether knocking down the *HERG* potassium channel in iPS-CMs would recapitulate a physiologically relevant cellular phenotype. We found that knocking down *HERG* in iPS-CMs lead to a prolonged beat duration and the appearance of a shoulder during the downstroke, as measured using the GCaMP signal (which can be used as a surrogate for the action potential) (Huebsch et al., 2015) (Figures 6D and 6E). We confirmed the prolongation of action potential duration by patch-clamp electrophysiology in the *HERG* knockdown samples (Figures 6F). We expected this result, because the *HERG* potassium channel pumps potassium ions out of cells to lower the inner membrane potential during diastole. This cellular phenotype recapitulates aspects of the phenotype observed in LQT patients and their iPS-CMs (Schwartz et al., 2012; Spencer et al., 2014).

DISCUSSION

In this study, we combined the power of human iPSC technology, which generates functional human cells, with inducible CRISPR-based genome editing and modulation technologies. Using the TetO inducible system, we deploy the newly developed CRISPRi system in the AAVS1 safe–harbor locus of human iPSCs to enable precise control of transcript silencing upon addition of doxycycline. With this approach, we rapidly and efficiently generated loss-of-function phenotypes in iPSCs and their cell-type derivatives to study mechanisms in development and disease. We introduced a single doxycycline-inducible vector system into the AAVS1 safe-harbor locus to gain tight transcriptional control of dCas9-KRAB (for CRISPRi) and Cas9 (for CRISPRn) for gene knockdown and knockout studies, respectively. This inducible vector system helped us precisely control the timing of knocking down the expression of target genes in a clonal iPSC line carrying the gRNA of interest. We were also able to efficiently target the CRISPRi vector into non-iPSC human cells (T-lymphocytes) and show efficient levels of transgene knockdown, which demonstrates the versatility of using the CRISPRi system in a wide range of cell types. This system can be readily targeted to other human cellular models in vitro and also to mouse models (Soriano, 1999) by exchanging the AAVS1-homology arms with the ROSA26-specific knockin arms.

We found that in iPSC populations, CRISPRi produced a homogeneous and rapid loss-of-function phenotype compared to CRISPRn. CRISPRi avoids potential complications associated with incomplete loss-of-function and gain-of-function phenotypes in cell populations produced by Cas9-induced hypomorphic alleles. Therefore, CRISPRi represents a powerful technology for repressing gene expression in bulk populations and especially when performing genome-scale phenotypic screens. Every CRISPRi iPSC that contained a target-specific gRNA

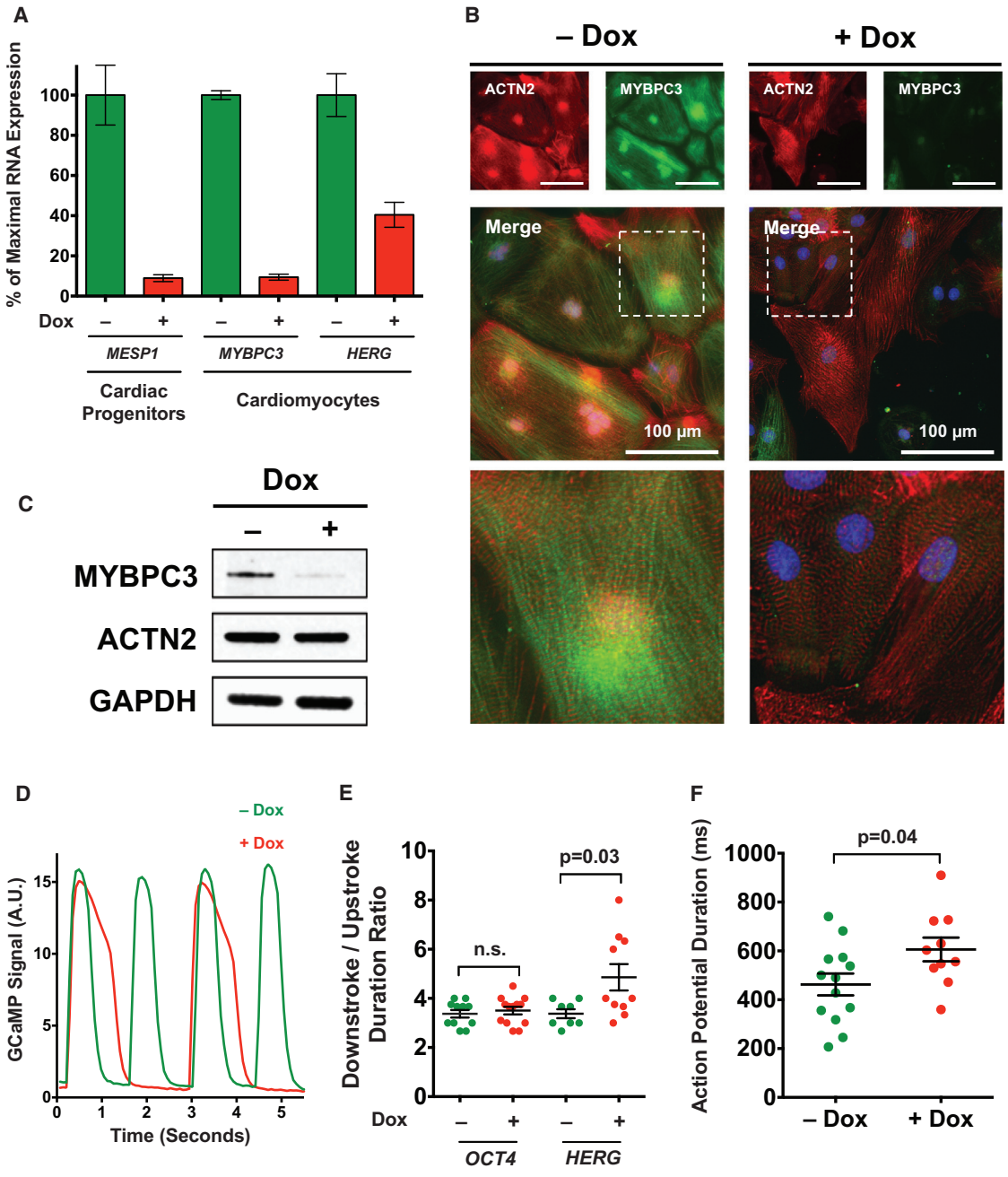

Figure 6. CRISPRi Knockdown in Differentiated Cell Types and Cardiac Disease Modeling

(A) Using CRISPRi, *MESP1* was knocked down by ~90% in polyclonal cardiac progenitors, and *MYBPC3* and *HERG* were knocked down by ~90% and 60% in polyclonal iPS-CMs, respectively.

(B) Immunostaining of day-35 lactate-purified iPS-CMs stained with antibodies against MYBPC3 (green) and ACTN2 (red). Using CRISPRi knockdown, loss of MYBPC3 was observed in over 85% of analyzed cells in a polyclonal population. Nuclei were counterstained with DAPI. Scale bar, 100 µm.

(C) Western blot of day-35 lactate-purified iPS-CMs with antibodies against MYBPC3, ACTN2, and GAPDH. Using CRISPRi, MYBPC3 protein was knocked down by ~90%.

(D) GCaMP fluorescence in iPS-CMs containing gRNA against *HERG* and cultured in doxycycline (red). Recordings show a prolonged beat duration compared to untreated controls (green).

(E) Quantified ratio of the downstroke-to-upstroke duration of doxycycline-treated iPS-CMs shows a significant difference in untreated iPS-CMs containing a gRNA against *HERG*, but not in iPS-CMs containing gRNA against *OCT4* (negative control).

(F) Patch-clamp recordings from single iPS-CMs show prolonged action potential durations in doxycycline-treated samples containing *HERG* gRNA.

Error bars represent SD.

displayed a rapid, uniform, and efficient transcriptional knockdown. This result was also validated across multiple endogenous loci in iPSCs, cardiac progenitors, and iPS-CMs. By contrast, using CRISPRn, we found that while all cells harbored the gRNA-expression vector and had continuous expression of Cas9, they did not all display complete loss-of-function phenotypes. Indeed, up to one-third of the cells maintained expression of the target gene. When we sequenced the target alleles, we found that of the mutated alleles, over one-third had in-frame INDELs, potentially resulting in a hypomorphic protein encoded by a gene that is now resistant to further Cas9 cutting using the target gRNA. Statistically, we expect that one-third of the INDELs generated by double-strand breaks induced by Cas9 through the non-homologous end-joining pathway would produce in-frame mutations. This effect could cause partial loss-of-function or gain-of-function phenotypes. Additionally, the location and size of the in-frame INDEL might not change the function of the mutated protein compared with the wild-type protein (Boettcher and McManus, 2015; Shi et al., 2015; Sung et al., 2013).

CRISPRi gRNAs were only effective at promoter regions close to the TSS, which may reduce the likelihood of off-target effects by transcriptional interference elsewhere in the genome. Indeed, RNA-seq analysis showed that the knockdown of GCaMP was highly specific. Furthermore, expression of dCas9-KRAB did not cause significant off-target transcriptional changes as compared to Cas9 expression alone. Although CRISPRi is highly effective, there are cases when other genetic tools such as CRISPRn, TALENs, and RNAi may have advantages. For instance, we and others (Gilbert et al., 2014) have shown that CRISPRi gRNAs are only effective near the TSS, which restricts the efficiency of transcript for genes that have poorly defined or multiple TSSs. CRISPRn and TALENs can be effective at any exon as long as the genomic region is accessible (Doench et al., 2014; Kim et al., 2013b). Additionally, RNAi can target any constitutive portion of the mRNA and has already been approved for human therapy (Davidson and McCray, 2011; Haussecker, 2012); however, RNAi has been shown to have many off-target effects (Jackson et al., 2003; Kim et al., 2013b; Krueger et al., 2007).

We also demonstrated the feasibility of allele-specific interference and the tunable nature of CRISPRi-based knockdown, which can be used to study the dose-dependent effects of a gene involved in development and disease. The dosage of transcription factors plays a significant role during development and organogenesis (McFadden et al., 2005; Takeuchi et al., 2011). In addition, many human diseases result from haploinsufficiency in which a mutation in a single copy of a gene produces the disease phenotype (Armanios et al., 2005; Marston et al., 2012; Minami et al., 2014; Theodoris et al., 2015). Therefore, to study the dose-dependent effects of transcription factors in development and disease, CRISPRi can be used to homogeneously tune the level of repression in cells by either choosing the relevant gRNA sequences or empirically titrating the levels of doxycycline to achieve the desired knockdown level. Alternatively, introducing a single point mutation at different positions in the gRNA sequence (which leads to mismatches between the RNA-DNA homology sequence) can be used to tune CRISPRi knockdown activity (Gilbert et al., 2014). Finally, CRISPRi knockdown was reversible in iPSCs upon doxycycline withdrawal, which would support studies involving transient knockdown of transcripts within a specific window during cell differentiation.

Our studies with CRISPRi in iPSCs showed that knocking down transcripts involved in maintaining pluripotency is highly efficient and rapidly causes a complete loss of pluripotent morphology, followed by cell differentiation in all cells expressing the appropriate gRNA. We also used this approach to knock down the *HERG* potassium channel to mimic an LQT2-type phenotype in iPS-CMs. We found that the inducible TetO promoter is partially silenced during the cardiac differentiation process, which has been reported to be due to methylation at CpG dinucleotides (Oyer et al., 2009). This silencing is independent of integration at the AAVS1 locus, as CAG-driven transgenes integrated at the AAVS1 locus remain active after differentiation. To avoid the effects of promoter silencing, we initiated transcript knockdown in the iPSC state or progenitor cells (day 5 of differentiation), where the vast majority of the cells respond to doxycycline. This strategy has proved highly effective at transgene knockdown in cardiac progenitors and iPS-CMs. To circumvent issues with silencing in future studies, we generated a non-inducible CRISPRi iPSC line (Gen3; in which dCas9-KRAB is driven off the CAG promoter), and the knockdown can be initiated upon introduction of gRNA. With this cell line, we expect to achieve highly efficient knockdown in differentiated cell types, such as iPS-CMs.

Several groups have used the CRISPR/Cas9 system for loss-of-function genetic screens in human cells (Shalem et al., 2014; Wang et al., 2014). Furthermore, some groups have used genome-scale screens with CRISPRi and CRISPR activation (CRISPRa) to identify known and novel genes that control cell growth and sensitivity to cholera-diphtheria toxin (Gilbert et al., 2014). In this study, we present our CRISPRi iPSC lines as suitable model systems for performing screens to identify novel transcripts of pluripotency, drug resistance, and cell survival at the pluripotent stem cell stage. With genome-scale screens, we can identify factors that improve cell-specific differentiation into functional cell types that have been traditionally hard to obtain, and we can more rapidly generate mature functional cell types that better mimic in vivo cell counterparts. In addition, with CRISPRi, we can repress putative disease-associated genes in a medium- to high-throughput manner to unravel the molecular mechanisms underlying human disease in vitro. Finally, we can build on the current power of CRISPRi for developmental screens by using an orthogonal dCas9-effector system for gene activation via CRISPRa, which can synergistically modulate gene knockdown and activation and direct cell fate toward a particular lineage.

EXPERIMENTAL PROCEDURES

iPSC Culture

WTB and WTC iPSCs and derivative lines were maintained under feeder-free conditions on growth factor-reduced Matrigel (BD Biosciences) and fed daily with mTeSR medium (STEMCELL Technologies) (Ludwig et al., 2006). Accutase (STEMCELL Technologies) was used to enzymatically dissociate iPSCs into single cells. To promote cell survival during enzymatic passaging, cells were passaged with the p160-Rho-associated coiled-coil kinase (ROCK) inhibitor Y-27632 (10 μM; Selleckchem) (Watanabe et al., 2007). iPSCs were frozen in 90% fetal bovine serum (HyClone) and 10%

DMSO (Sigma). The committee on Human Research at the University of California, San Francisco approved the iPSC research protocol (#10-02521).

Generation of Stable CRISPRi and CRISPRn iPSC Lines

iPSCs were singularized with accutase, resuspended in PBS, and counted with a Countess automated cell counter (Life Technologies). For plasmid transfections, the human stem cell nucleofector kit 1 solution was used on the Amaxa nucleofector 2b device (program A-23; Lonza). To generate the CRISPRi and CRISPRn iPSC lines, two million WTC or WTB iPSCs were nucleofected with the appropriate knockin vector (5 μg) and each AAVS1 TALEN pair (2 μg). Cells were then seeded in six-well plates in serial dilutions in mTeSR supplemented with Y-27632 (10 μM). Selection was applied 3 days post-nucleofection with the appropriate antibiotic in mTeSR plus Y-27632 (10 μM). To knock in the CRISPRi construct (carrying the Neomycin resistance gene cassette), Geneticin (Life Technologies) was applied at 100 μg/ml. To knock in the CRISPRn and GCaMP constructs (carrying the Puromycin resistance gene cassette), 0.5 μg/ml Puromycin (Life Technologies) was added. Selection was maintained for ~10 days until stable colonies appeared. Colonies with a diameter of greater than ~500 μm were manually picked using a P200 pipette tip under an EVOS FL picking microscope (Life Technologies) and transferred to individual wells of a 24-well plate containing mTeSR medium supplemented with Y-27632 (10 μM). Clones were then expanded into larger vessel formats.

Generation of CEM CRISPRi Cell Line

CEM CRISPRi cells were generated by electroporation of 0.5 μg of each AAVS1 TALEN pair and 1 μg of the Gen1 CRISPRi vector with an Amaxa nucleofector 2b device and Amaxa cell line nucleofector kit C (Lonza). Cells were selected in 1 μg/μl G418, and clonal lines were generated by dilution in 96-well plates. Clonal populations were selected based on doxycycline induction of mCherry expression. Oligos encoding the CD4 protospacer were annealed and cloned into the pSLQ1371 vector using restriction sites BstXI and BlpI, and lentivirus was produced in HEK293T cells (Gilbert et al., 2014). To compare performance of CD4 gRNAs, each was transduced into CEM-CRISPRi cells. Transduced populations were incubated for 96 hr with doxycycline (2 μM). Knockdown efficiency was calculated by gating all mCherry-expressing cells, and comparing cell-surface CD4 expression in the presence or absence of gRNA-expressing cells (BFP^+). Three independent stable CEM CRISPRi clones were selected with 0.6 μg/ml Puromycin and incubated in the presence or absence of doxycycline (2 μM) for 14 days to assess maximal CD4 knockdown. Cells were stained using anti-CD4 APC-conjugated antibody and cell surface CD4 staining was quantified using a BD LSRII flow cytometer. CD4 knockdown was quantified as percent reduction relative to no doxycycline treatment condition.

gRNA Design and Cloning into the gRNA-Expression Vector

For CRISPRi, three to five gRNAs were designed to target near the TSS of the gene of interest (250 bp upstream and downstream, respectively). The location of the TSS was determined using NCBI (http://www.ncbi.nlm.nih.gov/). gRNA oligos were designed, phosphorylated, annealed, and cloned into the pgRNA-CKB vector using BsmBI ligation strategy. Additional details and a list of gRNA sequences are listed in supplemental experimental procedures.

gRNA Nucleofection and Selection of Stable CRISPRi and CRISPRn Clones

The gRNA-expression vector (pgRNA-CKB) was transfected into either the CRISPRi or CRISPRn cells with the human stem cell nucleofector kit 1 solution on the Amaxa nucleofector 2b device (program A-23; Lonza). Two million CRISPRi or CRISPRn iPSCs and 5 μg of the circular gRNA-expression plasmid were used per nucleofection. Nucleofected cells were then seeded in a single well of a six-well plate in mTeSR supplemented with Y-27632 (10 μM). Blasticidin selection (10 μg/ml) was applied 24 hr post-nucleofection in mTeSR supplemented with Y-27632 (10 μM) for 7–10 days, until stable colonies appeared. Stable colonies were then pooled and passaged at least three times in mTeSR plus Blasticidin and Y-27632 to enrich for cells with integration at transcriptionally active sites (Figure S3).

RNA Sequencing

For each sample, 1 μg of total RNA was prepared using TRIzol as previously described. Strand-specific mRNAseq libraries were prepared using TruSeq Stranded mRNA Library Prep Kit (Illumina). Upon completion, libraries were quantified and pooled using Qubit dsDNA HS assay and Agilent's Bioanalyzer high-sensitivity DNA assay. The indexed libraries were pooled and sequenced on Illumina HiSeq 4000 as 50-bp single-end reads. Reads were aligned to the hg19 genome assembly using the Ensembl 75 reference transcriptome customized to include the GCaMP6f constructs using TopHat2 (Kim et al., 2013a). Unaligned reads were subsequently aligned to the CRISPRi or CRISPRn knockin constructs where appropriate. Transcript alignments were then counted using SubRead v1.4.6 and analyzed with custom scripts written in Python (Liao et al., 2013). All data are displayed as reads per million (RPM) with a pseudocount of 0.075.

iPS-CM Differentiation and Lactate Purification

iPSCs were differentiated into iPS-CMs using the WNT modulation-differentiation method (Lian et al., 2012) (Figure S5A). iPS-CMs were purified via a modified version of the lactate metabolic-selection method (Tohyama et al., 2013). Additional details are outlined in Supplemental Experimental Procedures.

ACCESSION NUMBERS

The accession number for the RNA-seq data reported in this paper is GEO: PRJNA307261.

SUPPLEMENTAL INFORMATION

Supplemental Information includes Supplemental Experimental Procedures, six figures, and one movie and can be found with this article online at http://dx.doi.org/10.1016/j.stem.2016.01.022.

AUTHOR CONTRIBUTIONS

M.A.M. and B.R.C. were primarily responsible for conception, design, and interpretation of the experiments. M.A.M. conducted most experiments with help from N.H., E.F., E.S., A.T., M.P.O., T.V.E., K.H., and L.M.J. Y.M. and A.H.C. generated the CRISPRn Gen1C iPSC line. C.I.S. performed electrophysiology experiments. D.E.G. generated the CEM CRISPRi cell line and provided knockdown analysis. L.A.G., J.S.W., and L.S.Q. provided technical expertise, the CRISPRi fusion cassette, and gRNA expression constructs. J.E.V. and M.A.H. conducted and analyzed the RNA-seq experiments. M.A.M., P.L.S., and B.R.C. wrote the manuscript with support from all authors.

ACKNOWLEDGMENTS

We thank members of the Conklin laboratory, Gladstone Institute of Cardiovascular Disease, Roddenberry Stem Cell Core, BioFulcrum, a Gladstone Institutes Enterprise, and Innovative Genomics Institute for technical assistance and helpful comments on the manuscript. We thank Tim Rand and Knut Woltjen for valuable discussions and helpful comments on the manuscript. We thank S. John Liu for RNA-seq analysis advice. We thank Jen Berman and Samantha Cooper at Bio-Rad for assistance with designing ddPCR probe-primer sets. Summer students Matthew Keller and Monique Morrison assisted with preliminary experiments. CEM $CD4^+$ cells were obtained from Dr. J.P. Jacobs through the AIDS Reagent Program, Division of AIDS, NIAID, NIH. M.A.M. is supported by the Canadian Institutes of Health Research postdoctoral fellowship 129844. N.H. was supported by the CIRM training program TG2-01160 and T32 HL007544. E.F. was supported by a Bridges to Stem Cell Training grant TB1-01188 from CIRM. L.M.J. is supported by the CIRM Training Grant TG2-01160 and NICHD Career Development Award 1K12HD072222. Y.M. received fellowships from the Uehara Memorial Foundation Research and Gladstone-CIRM. D.G. is supported by UCSF-Gladstone Center for AIDS Research (CFAR), an NIH-funded program (P30 AI027763). T.V.E. was supported by Carlsberg Travel Grant (2013-01-0423), The Lundbeck Foundation (R140-2013-13348), and OUH Internationalisation Foundation. J.E.V., M.A.H., L.A.G., and J.S.W. were supported by the Howard Hughes

Medical Institute and the National Institutes of Health (R01 DA036858). B.R.C. received support from the US National Heart, Lung, and Blood Institute, the National Institutes of Health (U01-HL100406, U01-GM09614, R01-HL108677, U01-HL098179, U01-HL099997, P01-HL089707, R01HL130533, and R01-HL060664), and an Agilent University Relations Grant.

Received: August 20, 2015
Revised: December 21, 2015
Accepted: January 24, 2016
Published: March 10, 2016

REFERENCES

Apáti, Á., Pászty, K., Hegedűs, L., Kolacsek, O., Orbán, T.I., Erdei, Z., Szebényi, K., Péntek, A., Enyedi, Á., and Sarkadi, B. (2013). Characterization of calcium signals in human embryonic stem cells and in their differentiated offspring by a stably integrated calcium indicator protein. Cell. Signal. *25*, 752–759.

Armanios, M., Chen, J.-L., Chang, Y.-P.C., Brodsky, R.A., Hawkins, A., Griffin, C.A., Eshleman, J.R., Cohen, A.R., Chakravarti, A., Hamosh, A., and Greider, C.W. (2005). Haploinsufficiency of telomerase reverse transcriptase leads to anticipation in autosomal dominant dyskeratosis congenita. Proc. Natl. Acad. Sci. USA *102*, 15960–15964.

Boettcher, M., and McManus, M.T. (2015). Choosing the Right Tool for the Job: RNAi, TALEN, or CRISPR. Mol. Cell *58*, 575–585.

Bolouri, H., and Davidson, E.H. (2003). Transcriptional regulatory cascades in development: initial rates, not steady state, determine network kinetics. Proc. Natl. Acad. Sci. USA *100*, 9371–9376.

Chen, T.-W., Wardill, T.J., Sun, Y., Pulver, S.R., Renninger, S.L., Baohan, A., Schreiter, E.R., Kerr, R.A., Orger, M.B., Jayaraman, V., et al. (2013). Ultrasensitive fluorescent proteins for imaging neuronal activity. Nature *499*, 295–300.

Cong, L., Ran, F.A., Cox, D., Lin, S., Barretto, R., Habib, N., Hsu, P.D., Wu, X., Jiang, W., Marraffini, L.A., and Zhang, F. (2013). Multiplex genome engineering using CRISPR/Cas systems. Science *339*, 819–823.

Davidson, B.L., and McCray, P.B., Jr. (2011). Current prospects for RNA interference-based therapies. Nat. Rev. Genet. *12*, 329–340.

Doench, J.G., Hartenian, E., Graham, D.B., Tothova, Z., Hegde, M., Smith, I., Sullender, M., Ebert, B.L., Xavier, R.J., and Root, D.E. (2014). Rational design of highly active sgRNAs for CRISPR-Cas9-mediated gene inactivation. Nat. Biotechnol. *32*, 1262–1267.

Doudna, J.A., and Charpentier, E. (2014). Genome editing. The new frontier of genome engineering with CRISPR-Cas9. Science *346*, 1258096.

Gaj, T., Gersbach, C.A., and Barbas, C.F., 3rd (2013). ZFN, TALEN, and CRISPR/Cas-based methods for genome engineering. Trends Biotechnol. *31*, 397–405.

Gilbert, L.A., Larson, M.H., Morsut, L., Liu, Z., Brar, G.A., Torres, S.E., Stern-Ginossar, N., Brandman, O., Whitehead, E.H., Doudna, J.A., et al. (2013). CRISPR-mediated modular RNA-guided regulation of transcription in eukaryotes. Cell *154*, 442–451.

Gilbert, L.A., Horlbeck, M.A., Adamson, B., Villalta, J.E., Chen, Y., Whitehead, E.H., Guimaraes, C., Panning, B., Ploegh, H.L., Bassik, M.C., et al. (2014). Genome-Scale CRISPR-Mediated Control of Gene Repression and Activation. Cell *159*, 647–661.

González, F., Zhu, Z., Shi, Z.-D., Lelli, K., Verma, N., Li, Q.V., and Huangfu, D. (2014). An iCRISPR platform for rapid, multiplexable, and inducible genome editing in human pluripotent stem cells. Cell Stem Cell *15*, 215–226.

Haussecker, D. (2012). The business of RNAi therapeutics in 2012. Mol. Ther. Nucleic Acids *1*, e8.

Hayashi, Y., Caboni, L., Das, D., Yumoto, F., Clayton, T., Deller, M.C., Nguyen, P., Farr, C.L., Chiu, H.-J., Miller, M.D., et al. (2015). Structure-based discovery of NANOG variant with enhanced properties to promote self-renewal and reprogramming of pluripotent stem cells. Proc. Natl. Acad. Sci. USA *112*, 4666–4671.

Hockemeyer, D., Wang, H., Kiani, S., Lai, C.S., Gao, Q., Cassady, J.P., Cost, G.J., Zhang, L., Santiago, Y., Miller, J.C., et al. (2011). Genetic engineering of human pluripotent cells using TALE nucleases. Nat. Biotechnol. *29*, 731–734.

Huebsch, N., Loskill, P., Mandegar, M.A., Marks, N.C., Sheehan, A.S., Ma, Z., Mathur, A., Nguyen, T.N., Yoo, J.C., Judge, L.M., et al. (2015). Automated video-based analysis of contractility and calcium flux in human-induced pluripotent stem cell-derived cardiomyocytes cultured over different spatial scales. Tissue Eng. Part C Methods *21*, 467–479.

Jackson, A.L., Bartz, S.R., Schelter, J., Kobayashi, S.V., Burchard, J., Mao, M., Li, B., Cavet, G., and Linsley, P.S. (2003). Expression profiling reveals off-target gene regulation by RNAi. Nat. Biotechnol. *21*, 635–637.

Kearns, N.A., Genga, R.M.J., Enuameh, M.S., Garber, M., Wolfe, S.A., and Maehr, R. (2014). Cas9 effector-mediated regulation of transcription and differentiation in human pluripotent stem cells. Development *141*, 219–223.

Kim, H., and Kim, J.-S. (2014). A guide to genome engineering with programmable nucleases. Nat. Rev. Genet. *15*, 321–334.

Kim, D., Pertea, G., Trapnell, C., Pimentel, H., Kelley, R., and Salzberg, S.L. (2013a). TopHat2: accurate alignment of transcriptomes in the presence of insertions, deletions and gene fusions. Genome Biol. *14*, R36.

Kim, Y., Kweon, J., Kim, A., Chon, J.K., Yoo, J.Y., Kim, H.J., Kim, S., Lee, C., Jeong, E., Chung, E., et al. (2013b). A library of TAL effector nucleases spanning the human genome. Nat. Biotechnol. *31*, 251–258.

Krueger, U., Bergauer, T., Kaufmann, B., Wolter, I., Pilk, S., Heider-Fabian, M., Kirch, S., Artz-Oppitz, C., Isselhorst, M., and Konrad, J. (2007). Insights into effective RNAi gained from large-scale siRNA validation screening. Oligonucleotides *17*, 237–250.

Lian, X., Hsiao, C., Wilson, G., Zhu, K., Hazeltine, L.B., Azarin, S.M., Raval, K.K., Zhang, J., Kamp, T.J., and Palecek, S.P. (2012). Robust cardiomyocyte differentiation from human pluripotent stem cells via temporal modulation of canonical Wnt signaling. Proc. Natl. Acad. Sci. USA *109*, E1848–E1857.

Liao, Y., Smyth, G.K., and Shi, W. (2013). The Subread aligner: fast, accurate and scalable read mapping by seed-and-vote. Nucleic Acids Res. *41*, e108.

Lombardo, A., Cesana, D., Genovese, P., Di Stefano, B., Provasi, E., Colombo, D.F., Neri, M., Magnani, Z., Cantore, A., Lo Riso, P., et al. (2011). Site-specific integration and tailoring of cassette design for sustainable gene transfer. Nat. Methods *8*, 861–869.

Ludwig, T.E., Bergendahl, V., Levenstein, M.E., Yu, J., Probasco, M.D., and Thomson, J.A. (2006). Feeder-independent culture of human embryonic stem cells. Nat. Methods *3*, 637–646.

Mali, P., Yang, L., Esvelt, K.M., Aach, J., Guell, M., DiCarlo, J.E., Norville, J.E., and Church, G.M. (2013). RNA-guided human genome engineering via Cas9. Science *339*, 823–826.

Marston, S., Copeland, O., Gehmlich, K., Schlossarek, S., and Carrier, L. (2012). How do MYBPC3 mutations cause hypertrophic cardiomyopathy? J. Muscle Res. Cell Motil. *33*, 75–80.

McFadden, D.G., Barbosa, A.C., Richardson, J.A., Schneider, M.D., Srivastava, D., and Olson, E.N. (2005). The Hand1 and Hand2 transcription factors regulate expansion of the embryonic cardiac ventricles in a gene dosage-dependent manner. Development *132*, 189–201.

Minami, S.S., Min, S.-W., Krabbe, G., Wang, C., Zhou, Y., Asgarov, R., Li, Y., Martens, L.H., Elia, L.P., Ward, M.E., et al. (2014). Progranulin protects against amyloid β deposition and toxicity in Alzheimer's disease mouse models. Nat. Med. *20*, 1157–1164.

Miyaoka, Y., Chan, A.H., Judge, L.M., Yoo, J., Huang, M., Nguyen, T.D., Lizarraga, P.P., So, P.-L., and Conklin, B.R. (2014). Isolation of single-base genome-edited human iPS cells without antibiotic selection. Nat. Methods *11*, 291–293.

Oyer, J.A., Chu, A., Brar, S., and Turker, M.S. (2009). Aberrant epigenetic silencing is triggered by a transient reduction in gene expression. PLoS ONE *4*, e4832.

Qi, L.S., Larson, M.H., Gilbert, L.A., Doudna, J.A., Weissman, J.S., Arkin, A.P., and Lim, W.A. (2013). Repurposing CRISPR as an RNA-guided platform for sequence-specific control of gene expression. Cell *152*, 1173–1183.

Schwartz, P.J., Crotti, L., and Insolia, R. (2012). Long-QT syndrome: from genetics to management. Circ Arrhythm Electrophysiol *5*, 868–877.

Shalem, O., Sanjana, N.E., Hartenian, E., Shi, X., Scott, D.A., Mikkelson, T., Heckl, D., Ebert, B.L., Root, D.E., Doench, J.G., et al. (2014). Genome-scale CRISPR-Cas9 knockout screening in human cells. Science *343*, 84–87.

Shi, J., Wang, E., Milazzo, J.P., Wang, Z., Kinney, J.B., and Vakoc, C.R. (2015). Discovery of cancer drug targets by CRISPR-Cas9 screening of protein domains. Nat. Biotechnol. *33*, 661–667.

Soriano, P. (1999). Generalized lacZ expression with the ROSA26 Cre reporter strain. Nat. Genet. *21*, 70–71.

Spencer, C.I., Baba, S., Nakamura, K., Hua, E.A., Sears, M.A.F., Fu, C.C., Zhang, J., Balijepalli, S., Tomoda, K., Hayashi, Y., et al. (2014). Calcium transients closely reflect prolonged action potentials in iPSC models of inherited cardiac arrhythmia. Stem Cell Reports *3*, 269–281.

Sterneckert, J.L., Reinhardt, P., and Schöler, H.R. (2014). Investigating human disease using stem cell models. Nat. Rev. Genet. *15*, 625–639.

Sung, Y.H., Baek, I.-J., Kim, D.H., Jeon, J., Lee, J., Lee, K., Jeong, D., Kim, J.-S., and Lee, H.-W. (2013). Knockout mice created by TALEN-mediated gene targeting. Nat. Biotechnol. *31*, 23–24.

Takahashi, K., Tanabe, K., Ohnuki, M., Narita, M., Ichisaka, T., Tomoda, K., and Yamanaka, S. (2007). Induction of pluripotent stem cells from adult human fibroblasts by defined factors. Cell *131*, 861–872.

Takeuchi, J.K., Lou, X., Alexander, J.M., Sugizaki, H., Delgado-Olguín, P., Holloway, A.K., Mori, A.D., Wylie, J.N., Munson, C., Zhu, Y., et al. (2011). Chromatin remodelling complex dosage modulates transcription factor function in heart development. Nat. Commun. *2*, 187.

Theodoris, C.V., Li, M., White, M.P., Liu, L., He, D., Pollard, K.S., Bruneau, B.G., and Srivastava, D. (2015). Human disease modeling reveals integrated transcriptional and epigenetic mechanisms of NOTCH1 haploinsufficiency. Cell *160*, 1072–1086.

Tohyama, S., Hattori, F., Sano, M., Hishiki, T., Nagahata, Y., Matsuura, T., Hashimoto, H., Suzuki, T., Yamashita, H., Satoh, Y., et al. (2013). Distinct metabolic flow enables large-scale purification of mouse and human pluripotent stem cell-derived cardiomyocytes. Cell Stem Cell *12*, 127–137.

Wang, T., Wei, J.J., Sabatini, D.M., and Lander, E.S. (2014). Genetic screens in human cells using the CRISPR/Cas9 system. Science *343*, 80–84.

Wang, T., Birsoy, K., Hughes, N.W., Krupczak, K.M., Post, Y., Wei, J.J., Lander, E.S., and Sabatini, D.M. (2015). Identification and characterization of essential genes in the human genome. Science *350*, 1096–1101.

Watanabe, K., Ueno, M., Kamiya, D., Nishiyama, A., Matsumura, M., Wataya, T., Takahashi, J.B., Nishikawa, S., Nishikawa, S., Muguruma, K., and Sasai, Y. (2007). A ROCK inhibitor permits survival of dissociated human embryonic stem cells. Nat. Biotechnol. *25*, 681–686.

Wiedenheft, B., Sternberg, S.H., and Doudna, J.A. (2012). RNA-guided genetic silencing systems in bacteria and archaea. Nature *482*, 331–338.

Cell Stem Cell, Volume *18*

Supplemental Information

CRISPR Interference Efficiently Induces Specific and Reversible Gene Silencing in Human iPSCs

Mohammad A. Mandegar, Nathaniel Huebsch, Ekaterina B. Frolov, Edward Shin, Annie Truong, Michael P. Olvera, Amanda H. Chan, Yuichiro Miyaoka, Kristin Holmes, C. Ian Spencer, Luke M. Judge, David E. Gordon, Tilde V. Eskildsen, Jacqueline E. Villalta, Max A. Horlbeck, Luke A. Gilbert, Nevan J. Krogan, Søren P. Sheikh, Jonathan S. Weissman, Lei S. Qi, Po-Lin So, and Bruce R. Conklin

Supplemental Information

CRISPR Interference Efficiently Induces Specific and Reversible Gene Silencing in Human iPSCs

Mohammad A. Mandegar, Nathaniel Huebsch, Ekaterina B. Frolov, Edward Shin, Annie Truong, Michael P. Olvera, Amanda H. Chan, Yuichiro Miyaoka, Kristin Holmes, C. Ian Spencer, Luke M. Judge, David E. Gordon, Tilde V. Eskildsen, Jacqueline E. Villalta, Max A. Horlbeck, Luke A. Gilbert, Nevan J. Krogan, Søren P. Sheikh, Jonathan S. Weissman, Lei S. Qi, Po-Lin So, Bruce R. Conklin

Figure S1	**Derivation and validation of CRISPRi and CRISPRn iPSCs. Related to Figure 1.**
Figure S2	**Characterization and doxycycline response of lead CRISPRi and CRISPRn iPSCs. Related to Figure 1.**
Figure S3	**Comparison of efficiency of CRISPRi knockdown and CRISPRn knockout. Related to Figure 2.**
Figure S4	**gRNA knockdown efficiency. Related to Figure 3.**
Figure S5	**Tuning CRISPRi knockdown by titrating doxycycline concentration. Related to Figure 4.**
Figure S6	**Differentiation, purification, and doxycycline response of iPS-CMs. Related to Figure 6.**
Video S1	**Video of CRISPRi iPS-CMs under the GFP channel showing the calcium waves caused by the GCaMP fluorescent signal. Related to Figure 6.**

Figure S1

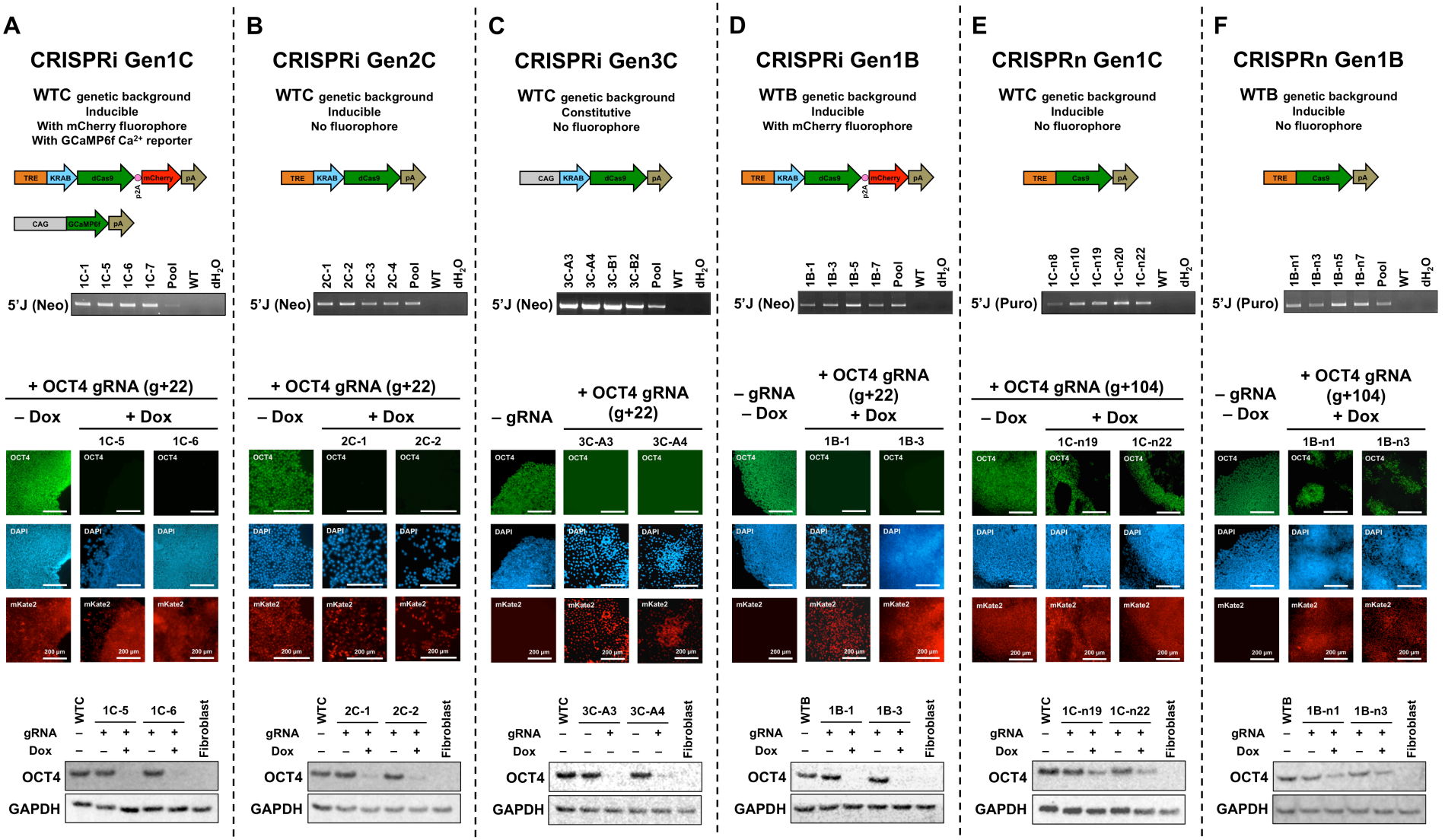
A
CRISPRi Gen1C
WTC genetic background
Inducible
With mCherry fluorophore
With GCaMP6f Ca2+ reporter
TRE
KRAB
dCas9
mCherry
p2A
pA
CAG
GCaMP6f
1C-1
1C-5
1C-6
1C-7
Pool
WT
dH2O
5'J (Neo)
+ OCT4 gRNA (g+22)
– Dox
+ Dox
1C-5
1C-6
OCT4
DAPI
mKate2
200 µm
WTC
gRNA
Dox
Fibroblast
GAPDH
B
CRISPRi Gen2C
WTC genetic background
Inducible
No fluorophore
2C-1
2C-2
2C-3
2C-4
5'J (Neo)
+ OCT4 gRNA (g+22)
C
CRISPRi Gen3C
WTC genetic background
Constitutive
No fluorophore
CAG
3C-A3
3C-A4
3C-B1
3C-B2
– gRNA
+ OCT4 gRNA (g+22)
D
CRISPRi Gen1B
WTB genetic background
Inducible
With mCherry fluorophore
1B-1
1B-3
1B-5
1B-7
– gRNA – Dox
+ OCT4 gRNA (g+22) + Dox
E
CRISPRn Gen1C
WTC genetic background
Inducible
No fluorophore
Cas9
1C-n8
1C-n10
1C-n19
1C-n20
1C-n22
5'J (Puro)
+ OCT4 gRNA (g+104)
F
CRISPRn Gen1B
WTB genetic background
Inducible
No fluorophore
1B-n1
1B-n3
1B-n5
1B-n7

Figure S1. Derivation and validation of CRISPRi and CRISPRn iPSCs. Related to Figure 1

(A-F) Schematic diagrams show CRISPRi and CRISPRn targeting constructs used in two different iPSC genetic backgrounds (WTC and WTB). Multiple clones from each targeting event were isolated. A subset of putative clones and a pooled population from each condition were analyzed using junction PCR and confirmed on-target integration of the cassette into the AAVS1 locus. Two putative clones from each condition were initially tested in polyclonal populations containing an OCT4-specific gRNA. Samples were either cultured in the presence or absence of doxycycline (2 μM) for 7 days and analyzed using immunocytochemistry. Nuclei were counterstained with DAPI. Clones were also analyzed using western blot with an antibody against OCT4, and GAPDH was used as a loading control. Scale bars = 200 μm.

Figure S2

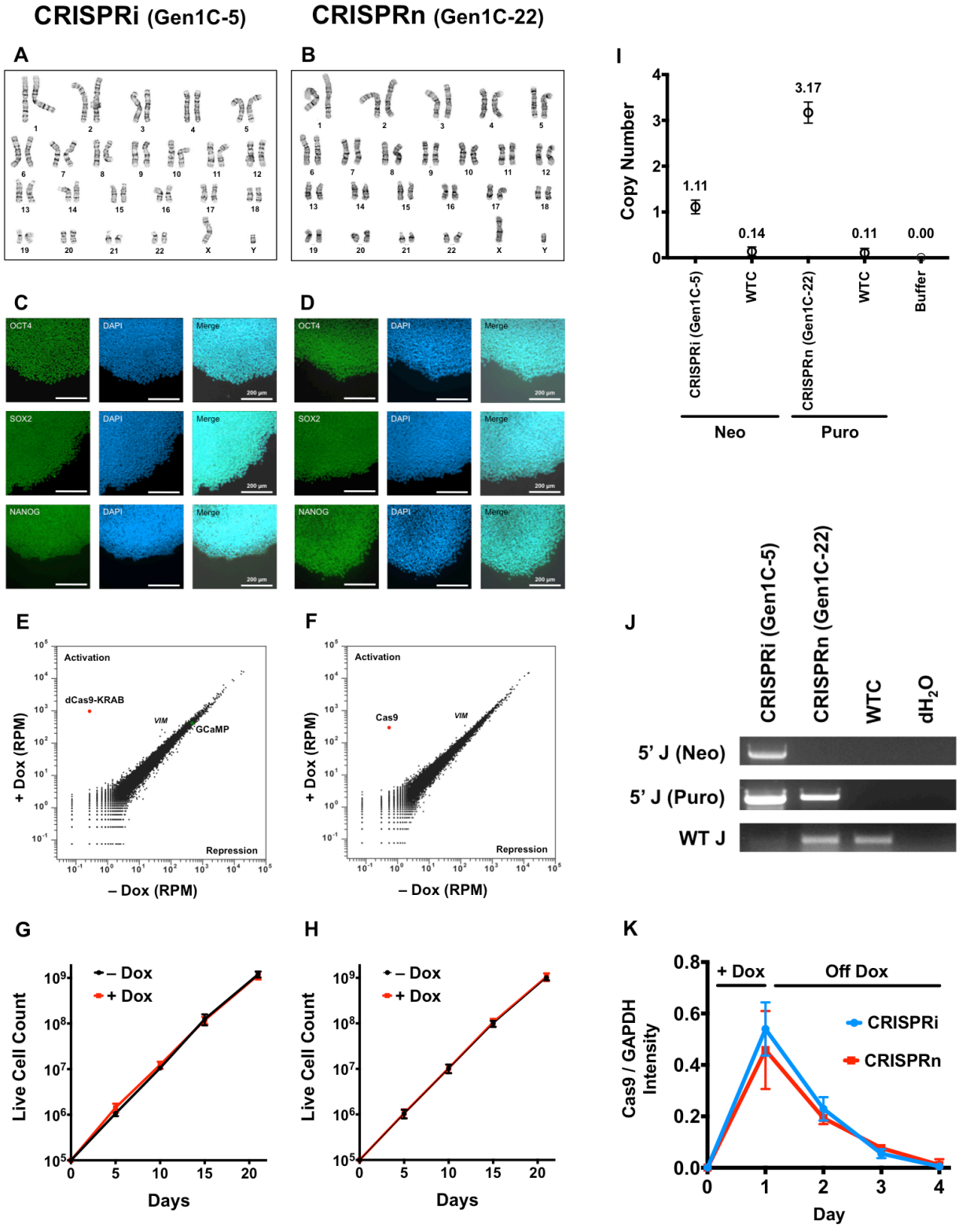
CRISPRi (Gen1C-5)
CRISPRn (Gen1C-22)
A
B
C
D
OCT4
SOX2
NANOG
DAPI
Merge
200 µm
E
F
Activation
dCas9-KRAB
VIM
GCaMP
Repression
+ Dox (RPM)
– Dox (RPM)
Cas9
G
H
– Dox
+ Dox
Live Cell Count
Days
I
Copy Number
1.11
0.14
3.17
0.11
0.00
CRISPRi (Gen1C-5)
WTC
CRISPRn (Gen1C-22)
WTC
Buffer
Neo
Puro
J
CRISPRi (Gen1C-5)
CRISPRn (Gen1C-22)
WTC
dH2O
5' J (Neo)
5' J (Puro)
WT J
K
+ Dox
Off Dox
CRISPRi
CRISPRn
Cas9 / GAPDH Intensity
Day

Figure S2. Characterization and doxycycline response of lead CRISPRi and CRISPRn iPSCs. Related to Figure 1.

(A, B) Karyotyping of lead CRISPRi (Gen1C 5) and CRISPRn (Gen1C 22) iPSC clones showed both lines are normal. Autosomal and sex chromosomes are annotated. (C, D) Immunostaining of CRISPRi and CRISPRn lines with pluripotency markers OCT4, SOX2, and NANOG (all in green), respectively. Nuclei were counterstained with DAPI. All cells expressed the pluripotency markers, indicating that they maintained their pluripotency after genetic modification. RNA-sequencing RPM (reads per million) are plotted for (E) CRISPRi and (F) CRISPRn iPSC, before and after 7 days of doxycycline treatment (2 μM). Expression profiles show robust induction of dCas9-KRAB and Cas9 with few off-target changes. Data is representative of two independent biological replicates. (G, H) CRISPRi and CRISPRn iPSCs were cultured with doxycycline for 3 weeks (4 passages). There were no adverse effects of dCas9-KRAB or Cas9 expression on the proliferative potential of iPSCs. (I) Droplet digital PCR (ddPCR) was used to identify the total number of transgene integration events for CRISPRi and CRISPRn clones with Neomycin- and Puromycin-specific probes, respectively. (J) Junction PCR confirmed on-target integration into the AAVS1 locus of the CRISPRi and CRISPRn clones. The CRISPRi clone also contains the GCaMP expression cassette at the other AAVS1 allele. (K) Intensity analysis of dCas9-KRAB and Cas9 was performed on two independent western blots normalizing the dCas9-KRAB and Cas9 signal intensity to GAPDH using ImageJ. Both the CRISPRi and CRISPRn clones have similar induction profiles. Error bars, SD. Scale bars = 200 μm.

Figure S3

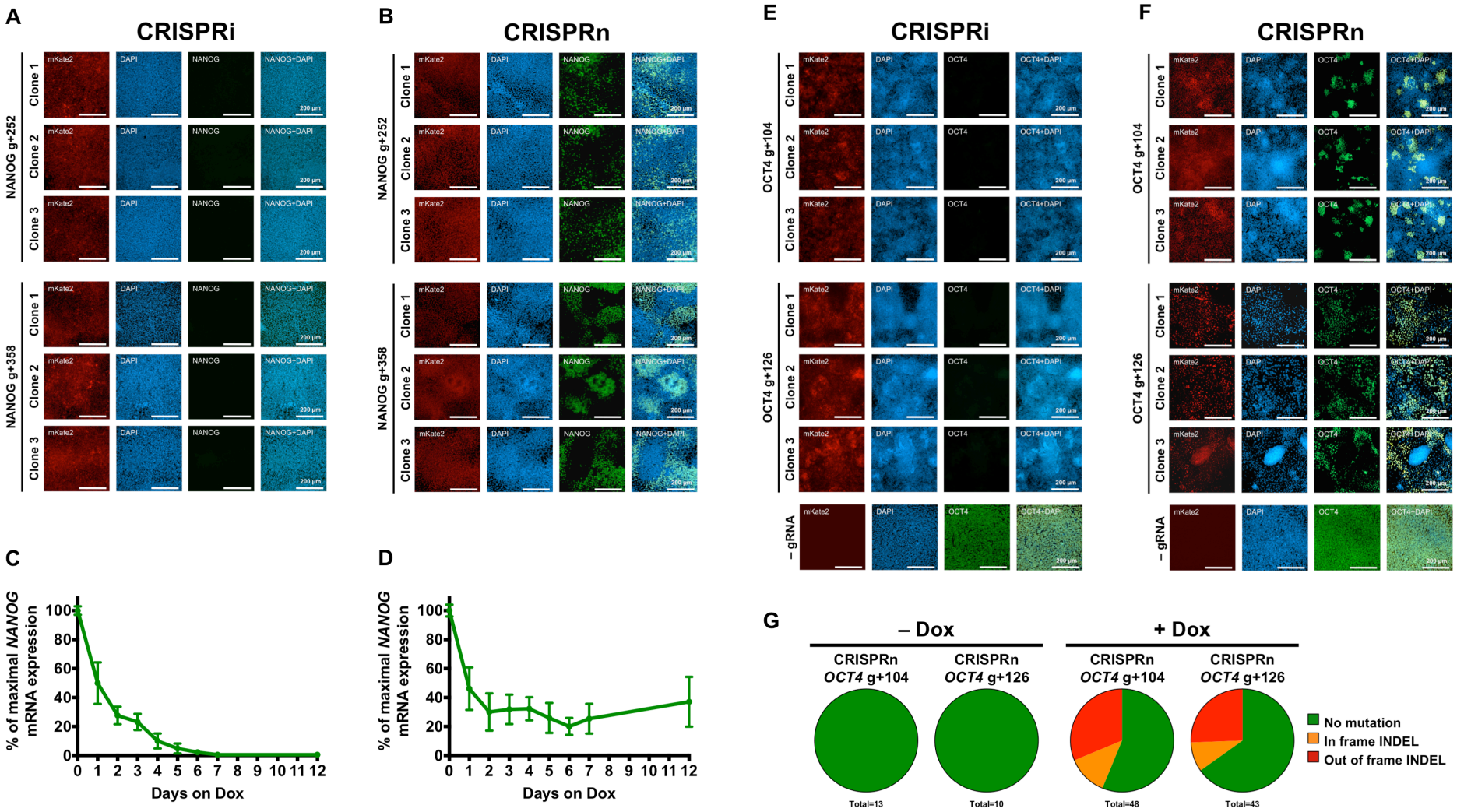
A
CRISPRi
B
CRISPRn
E
CRISPRi
F
CRISPRn
NANOG g+252
NANOG g+358
OCT4 g+104
OCT4 g+126
Clone 1
Clone 2
Clone 3
– gRNA
mKate2
DAPI
NANOG
NANOG+DAPI
OCT4
OCT4+DAPI
200 µm
C
D
% of maximal NANOG mRNA expression
Days on Dox
G
– Dox
+ Dox
CRISPRn OCT4 g+104
CRISPRn OCT4 g+126
Total=13
Total=10
Total=48
Total=43
No mutation
In frame INDEL
Out of frame INDEL

Figure S3. Comparison of efficiency of CRISPRi knockdown and CRISPRn knockout. Related to Figure 2.

Immunostaining of three independently-derived (A) CRISPRi and (B) CRISPRn colonies, containing different gRNAs (g+252 and g+358) against the first exon of *NANOG*. All CRISPRi gRNA-containing colonies showed complete knockdown of the target gene, while virtually all CRISPRn colonies showed variegated pattern of *NANOG* knockout. The mKate2 signal highlights the integration of the gRNA-expressing vector in all the cells within each clone. Nuclei were counterstained with DAPI. (C) qPCR analysis of CRISPRi cells show gradual loss of NANOG mRNA levels post initiation of knockdown. (D) For CRISPRn, mRNA levels rapidly drop within 2–3 days of knockout induction, however, remain stable thereafter. Immunostaining of three independently-derived stable (E) CRISPRi and (F) CRISPRn colonies containing different gRNAs (g+104 and g+126) against the first exon of *OCT4*. Using CRISPRi, *OCT4* expression was completely lost by 7 days post-doxycycline induction. While using CRISPRn, *OCT4* showed a variegated pattern of knockout and was expressed in 20-30% of the cells 7 days post-doxycycline induction. The mKate2 signal shows the presence of gRNA-expressing vector in all the cells. Nuclei were counterstained with DAPI. (G) Stable CRISPRn clones containing *OCT4* gRNA+104 and gRNA+126 were subjected to continuous doxycycline treatment for 14 days. Genomic DNA was extracted from non-doxycycline- and continuously doxycycline-treated cells and subjected to DNA sequencing. Even after 14 days of continuous doxycycline treatment, 55–65% of sequenced alleles contained no mutation and 30–40% of mutated alleles were in-frame INDELs. Red, out-of-frame INDELs; orange, in-frame INDELs; green, non-mutated alleles. The total number of sequenced colonies is listed below each pie graph. Error bars, SD. Scale bars = 200 μm.

Figure S4

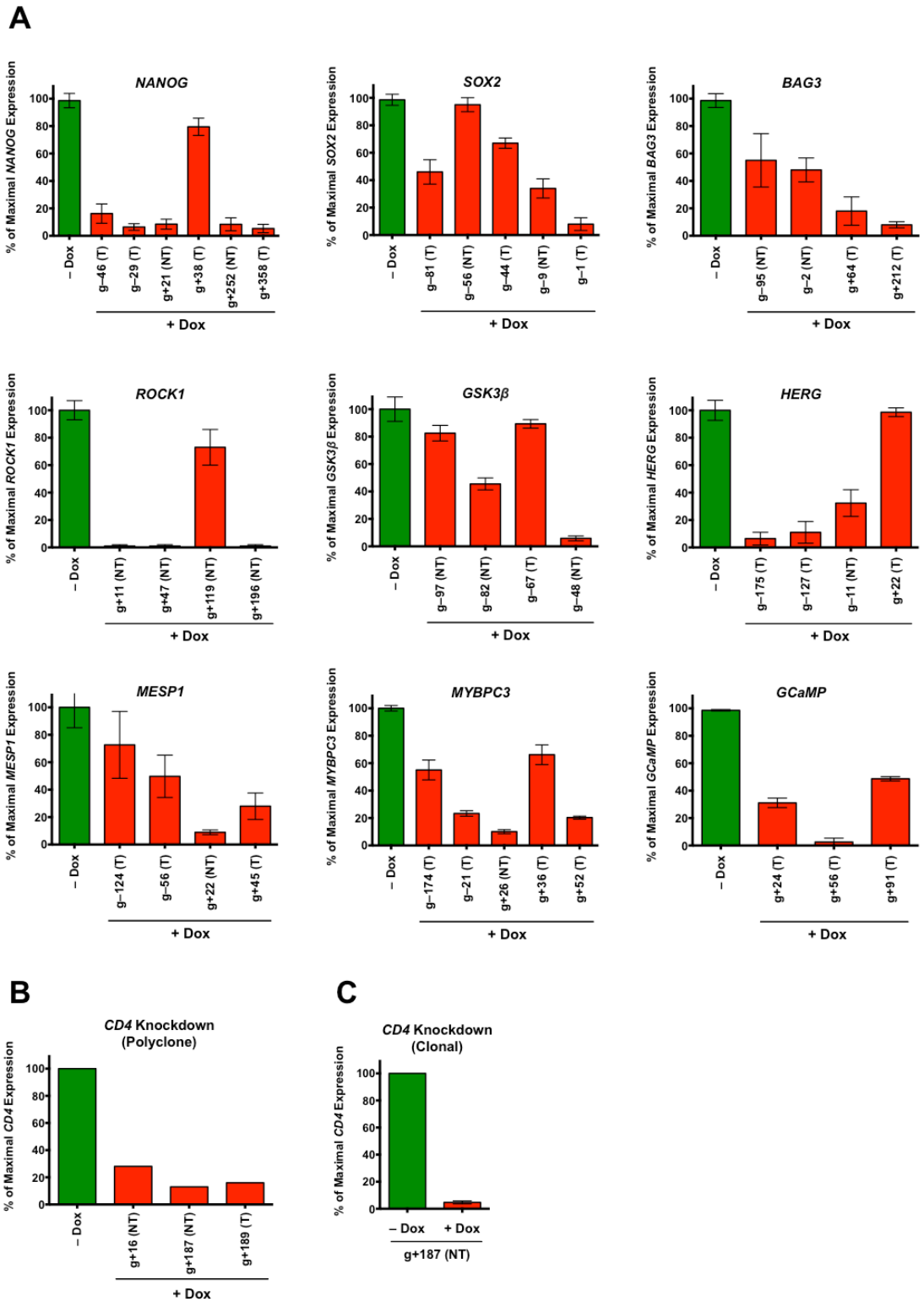
A
NANOG
% of Maximal NANOG Expression
– Dox
g–46 (T)
g–29 (T)
g+21 (NT)
g+38 (T)
g+252 (NT)
g+358 (T)
+ Dox
SOX2
% of Maximal SOX2 Expression
– Dox
g–81 (T)
g–56 (NT)
g–44 (T)
g–9 (NT)
g–1 (T)
+ Dox
BAG3
% of Maximal BAG3 Expression
– Dox
g–95 (NT)
g–2 (NT)
g+64 (T)
g+212 (T)
+ Dox
ROCK1
% of Maximal ROCK1 Expression
– Dox
g+11 (NT)
g+47 (NT)
g+119 (NT)
g+196 (NT)
+ Dox
GSK3β
% of Maximal GSK3β Expression
– Dox
g–97 (NT)
g–82 (NT)
g–67 (T)
g–48 (NT)
+ Dox
HERG
% of Maximal HERG Expression
– Dox
g–175 (T)
g–127 (T)
g–11 (NT)
g+22 (T)
+ Dox
MESP1
% of Maximal MESP1 Expression
– Dox
g–124 (T)
g–56 (T)
g+22 (NT)
g+45 (T)
+ Dox
MYBPC3
% of Maximal MYBPC3 Expression
– Dox
g–174 (T)
g–21 (T)
g+26 (NT)
g+36 (T)
g+52 (T)
+ Dox
GCaMP
% of Maximal GCaMP Expression
– Dox
g+24 (T)
g+56 (T)
g+91 (T)
+ Dox
B
CD4 Knockdown
(Polyclone)
% of Maximal CD4 Expression
– Dox
g+16 (NT)
g+187 (NT)
g+189 (T)
+ Dox
C
CD4 Knockdown
(Clonal)
% of Maximal CD4 Expression
– Dox
+ Dox
g+187 (NT)

Figure S4. gRNA knockdown efficiency. Related to Figure 3.
Three to five gRNAs were designed and tested in polyclonal (A) iPSC and (B) CEM cell populations. In iPSCs, knockdown efficiency was tested using qPCR (except for GCaMP knockdown efficiency which was measured using flow cytometry). For CEM cells, the knockdown efficiency was measured using flow cytometry. The binding location of each gRNA is indicated relative to the TSS of the gene of interest and whether it targets the template (T) or non-template (NT) strand. (C) Three independent CEM clonal lines containing CD4 g+187 were isolated and assayed for CRISPRi knockdown. Each data point is an average of 2–4 technical replicates. Error bars, SD.

Figure S5

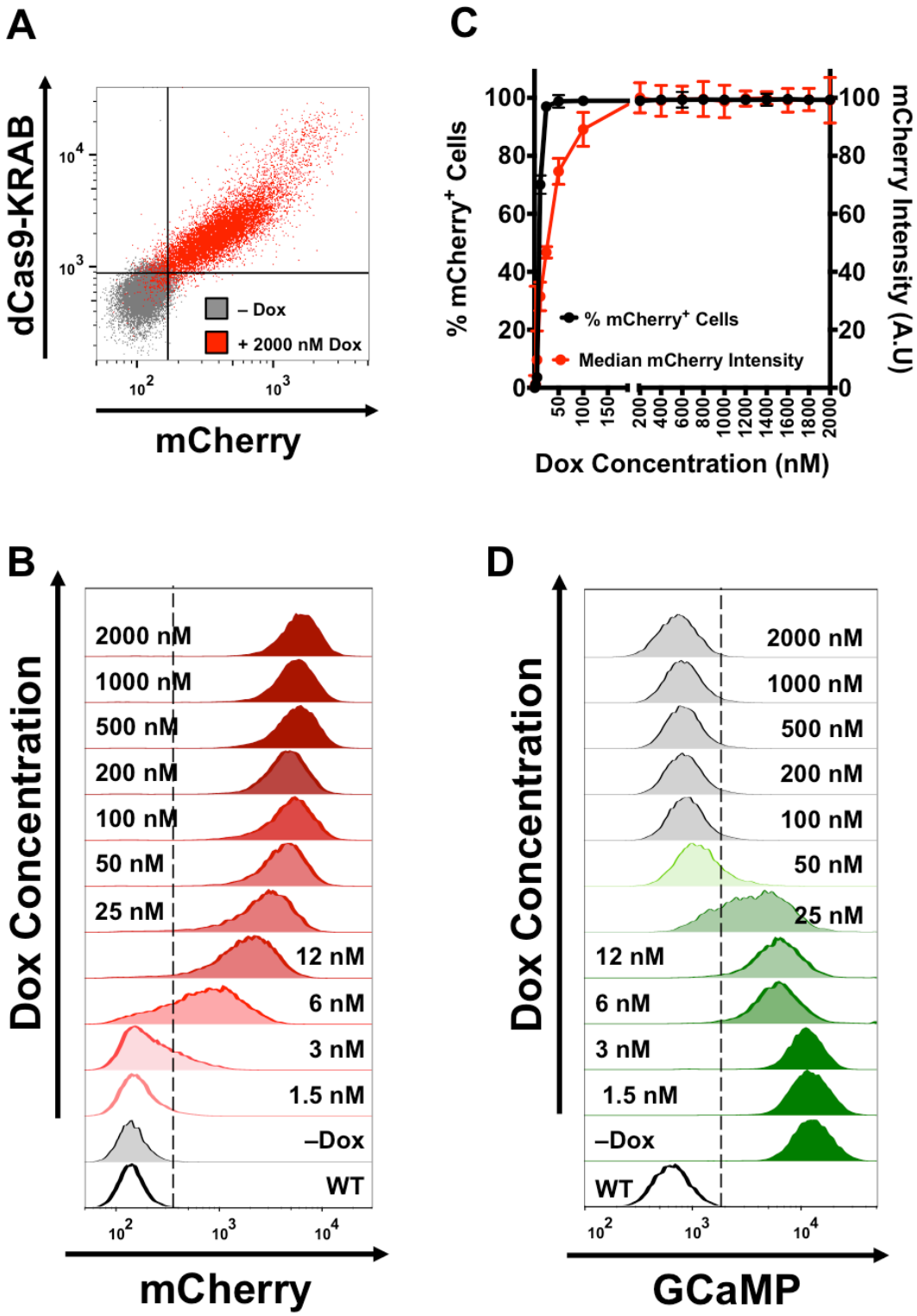
A
dCas9-KRAB
mCherry
– Dox
+ 2000 nM Dox
C
% mCherry+ Cells
mCherry Intensity (A.U)
% mCherry+ Cells
Median mCherry Intensity
Dox Concentration (nM)
B
Dox Concentration
2000 nM
1000 nM
500 nM
200 nM
100 nM
50 nM
25 nM
12 nM
6 nM
3 nM
1.5 nM
–Dox
WT
mCherry
D
Dox Concentration
GCaMP

Figure S5. Tuning CRISPRi knockdown by titrating doxycycline concentration. Related to Figure 4.

(A) Flow cytometry scatterplot of CRISPRi iPSCs treated with 2 μM of doxycycline shows dCas9-KRAB and mCherry are expressed at proportional levels (translated from a bicystronic transcript). (B) mCherry expression was measured using flow cytometery to test the response of the CRISPRi cells to various doses of doxycycline. (C) The percentage of mCherry-positive cells and mCherry fluorescent intensity as measured by the median fluorescent intensity) were plotted at different doxycycline concentrations. As a single copy, the TetO promoter behaves similar to a binary switch and only within a narrow range of doxycycline concentration, the expression can be robustly tuned. (D) By titrating the dose of doxycycline, GCaMP expression levels could be tuned within a narrow range (3-12 nM). Flow cytometry plots representative of three biological replicates. Error bars, SD.

Figure S6

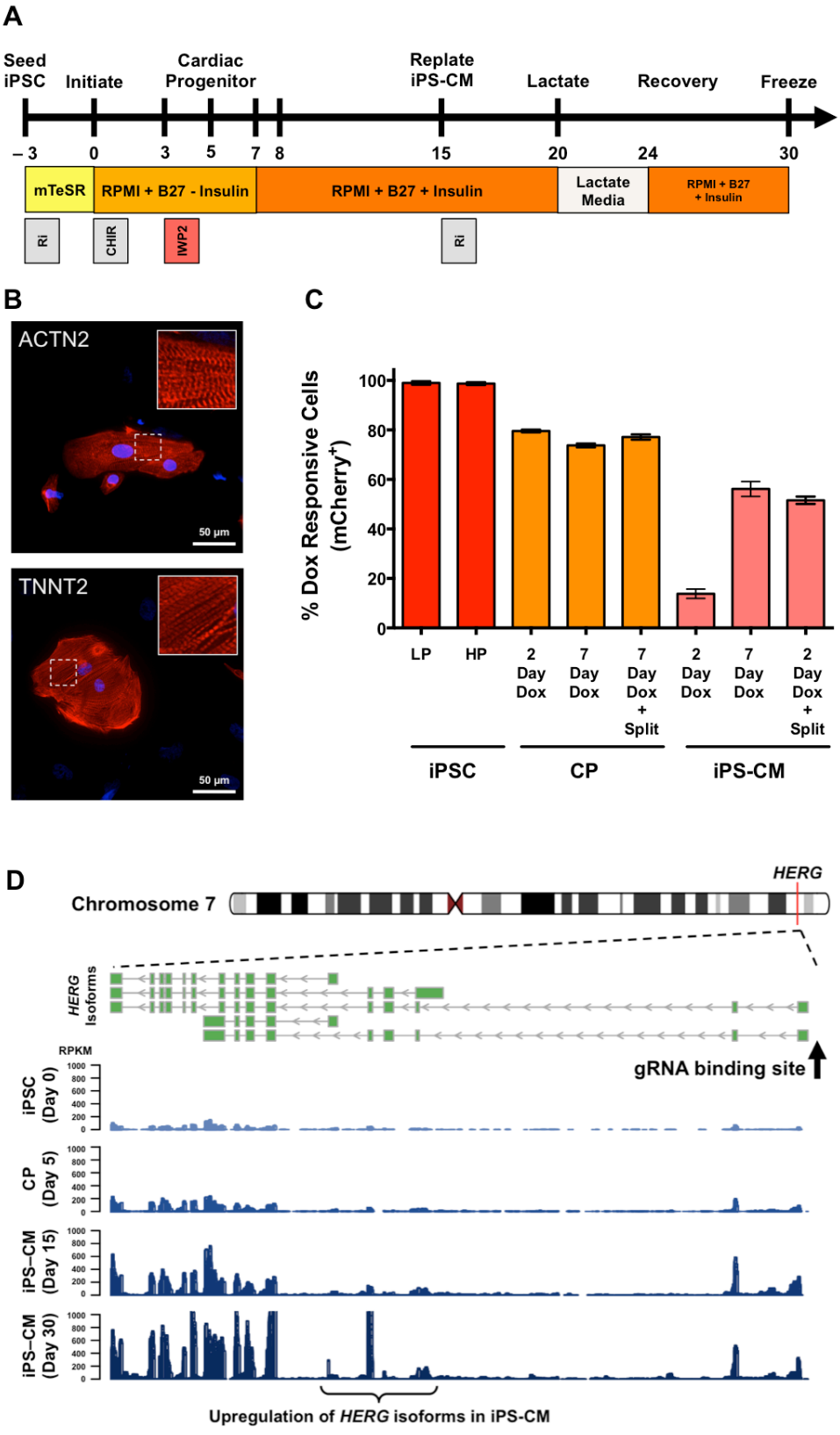
A
Seed iPSC
Initiate
Cardiac Progenitor
Replate iPS-CM
Lactate
Recovery
Freeze
– 3
0
3
5
7
8
15
20
24
30
mTeSR
RPMI + B27 - Insulin
RPMI + B27 + Insulin
Lactate Media
RPMI + B27 + Insulin
Ri
CHIR
IWP2
Ri
B
ACTN2
50 µm
TNNT2
50 µm
C
% Dox Responsive Cells (mCherry+)
100
80
60
40
20
0
LP
HP
2 Day Dox
7 Day Dox
7 Day Dox + Split
2 Day Dox
7 Day Dox
2 Day Dox + Split
iPSC
CP
iPS-CM
D
Chromosome 7
HERG
HERG Isoforms
RPKM
gRNA binding site
iPSC (Day 0)
CP (Day 5)
iPS–CM (Day 15)
iPS–CM (Day 30)
1000
800
600
400
200
0
Upregulation of HERG isoforms in iPS-CM

Figure S6. Differentiation, purification and doxycycline response of iPS-CMs. Related to Figure 6.

(A) Schematic diagram of the modified WNT-differentiation protocol for iPS-derived cardiomyocyte (iPS-CM) differentiation, lactate purification, and cryopreservation. (B) Lactate-purified iPS-CMs were stained with sarcomeric-specific markers ACTN2 and TNNT2. (C) Flow cytometry was used to measure doxycycline responsiveness (using mCherry expression) of low-passage (LP) and high-passage (HP; 3 months in culture) iPSC, cardiac progenitors (CP; day 5) and iPS-derived cardiomyocyte (iPS-CM; day 15) CRISPRi cells. Both low and high passage iPSC fully respond to doxycycline. 75-80% of cardiac progenitors cells respond to doxycycline. Less than 20% of iPS-CM responded to doxycycline after 2 days of treatment, while increasing the duration of doxycycline treatment to 7 days increases the percentage of responsive cells. Furthermore, only 2 days of doxycycline treatment with splitting the cells enabled more than 50% of the cells to respond. This indicates that the differentiated cells are prone to silencing at the TetO promoter. (D) RNA-Seq reads from the *HERG* transcript isoforms during iPS-CM differentiation. An arrow indicates the gRNA binding location, which targets the major transcript expressed in iPSCs. During cardiac differentiation, activation of the other isoforms (indicated by a bracket) is observed. Error bars, SD. Scale bars = 50 μm.

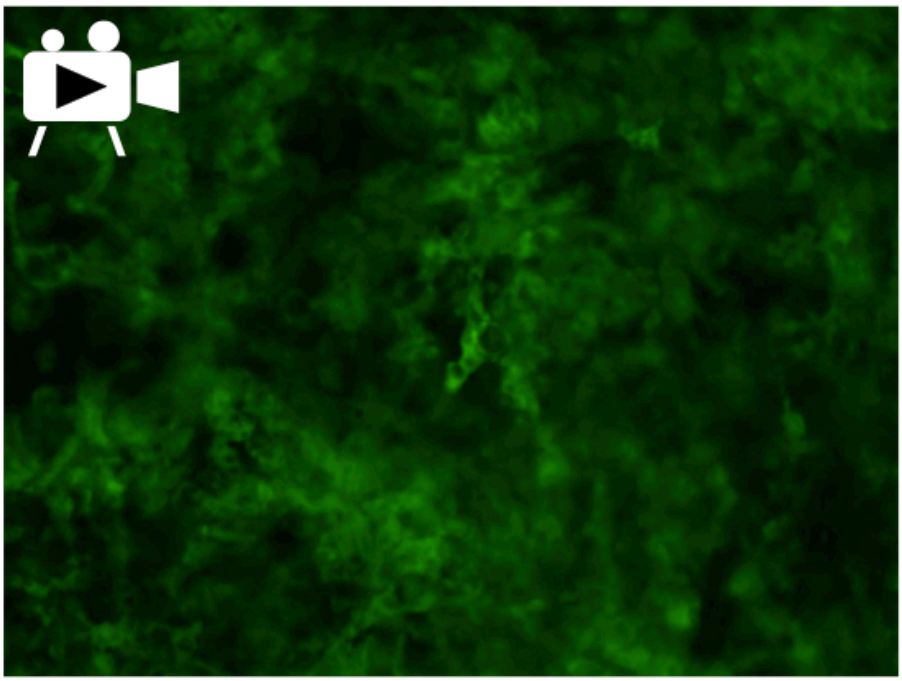

Video S1. Video of CRISPRi iPS-CMs under the GFP channel showing the calcium waves caused by the GCaMP fluorescent signal. Related to Figure 6.

Supplemental Experimental Procedures

iPSC Culture

Episomal reprogramming (Okita et al., 2011) was used to reprogram dermal fibroblasts from a healthy male and female individual to wild-type C (WTC) and wild-type B (WTB) human iPSC, respectively. The committee on Human Research at the University of California, San Francisco (UCSF) approved the iPSC-research protocol (#10-02521).

CRISPRi, CRISPRn, and GCaMP6f AAVS1 Knock-In Vectors

To generate iPSC lines with inducible CRISPR interference (CRISPRi) and CRISPR nuclease (CRISPRn), a single tetracycline-inducible vector was constructed to contain both the reverse tetracycline-controlled transcriptional activator (rtTA) and the tetracycline-response element (TRE3G). A strong constitutive promoter (CAG) transcribes rtTA and is oriented in the opposite direction of TRE3G element to ensure no leaky expression of the transgene without doxycycline. The TetO promoter transcribes dCas9-KRAB-P2A-mCherry (CRISPRi Gen1), dCas9-KRAB (CRISPRi Gen2) or Cas9 (CRISPRn Gen1). In the non-inducible CRISPRi clones (CRISPRi Gen3) dCas9-KRAB is expressed from the constitutive CAG promoter. In all CRISPRi lines, the KRAB domain is fused at the N-terminus of dCas9 (Gilbert et al., 2014). All CRISPRi and CRISPRn targeting vectors contained left- and right-homology arms (~800 bp) that flank the genomic-cut site in the AAVS1 locus. The vectors also contained a splice-acceptor (SA) site followed by the open reading frame (ORF) of a promoterless T2A-neomycin or T2A-puromycin resistance gene cassette, respectively (Figures 1A and 1B). The GCaMP6f knock-in vector that is specific for AAVS1 contains ~800 bp left and right of the AAVS1-homology arms, an SA site followed by the ORF of a promoterless T2A-puromycin resistance gene, and the GCaMP6f ORF driven off the CAG promoter (Figure 4).

Description of vectors

Vector Name **(Size)**	**Description & Addgene ID**	**Promoter** **Transgene of interest**	**Promoter** **Mammalian Resistance Gene**	**Bacterial Resistance Gene**
AAVS1 TALEN F (8,345 bp)	Homodimeric AAVS1 TALEN right pair	CMV RVD-FOK1	SV40 *Neo*^{R}	*Amp* and *Kan*
AAVS1 TALEN R (8,345 bp)	Homodimeric AAVS1 TALEN left pair	CMV RVD-FOK1	SV40 *Neo*^{R}	*Amp* and *Kan*
pAAVS1-NDi-CRISPRi (Gen1) (13,834 bp)	Dox-inducible CRISPR interference (CRISPRi) knock in construct into the AAVS1 locus with mCherry marker	TetO (TRE3G) dCas9-KRAB P2A mCherry	Endogenous AAV *Neo*^{R}	*Amp*

	(Gen1 CRISPRi vector)	(KRAB domain is fused at the N-terminus of dCas9)		
pAAVS1-NDi-CRISPRi (Gen2) (13,069 bp)	Dox-inducible CRISPR interference (CRISPRi) knock in construct into the AAVS1 locus (Gen2 CRISPRi vector)	TetO (TRE3G) dCas9-KRAB (KRAB domain is fused at the N-terminus of dCas9)	Endogenous AAV *Neo^R*	*Amp*
pAAVS1-NC-CRISPRi (Gen3) (11,437 bp)	Constitutive CRISPR interference (CRISPRi) knock in construct into the AAVS1 locus (Gen3 CRISPRi vector) Addgene ID: 73499	CAG dCas9-KRAB (KRAB domain is fused at the N-terminus of dCas9)	Endogenous AAV *Neo^R*	*Amp*
pAAVS1-PDi-CRISPRn (12,658 bp)	Dox-inducible CRISPR nuclease (CRISPRn) knock in construct into the AAVS1 locus	TetO (TRE3G) spCas9	Endogenous AAV *Puro^R (Pac)*	*Amp*
pgRNA-CKB (9,596 bp)	Guide RNA expression vector (with mKate2) Addgene ID: 73501	CAG NLS-mKate2-T2A-Bsd Mouse U6 gRNA	CAG *Bsd^R (Bsr)*	*Amp*
pgRNA-CGB (9,617 bp)	Guide RNA expression vector (with GFP) Addgene ID: 73502	CAG NLS-GFP-T2A-Bsd Mouse U6 gRNA	CAG *Bsd^R* (Bsr)	*Amp*
pAAVS1-PC-GCaMP6f (8,007 bp)	GCaMP knock in construct into the AAVS1 locus Addgene ID: 73503	CAG GCaMP6f	Endogenous AAV Puro^R (Pac)	*Amp*

gRNA Design and Cloning into the gRNA-Expression Vector

If empirical data were available based on RNAseq or cDNA sequences from iPSC and iPS-CM, those were given priority over the NCBI database. For CRISPRn, up to three gRNAs were designed to target within the first common exon of the gene of interest with a minimal number of off-target sites in the genome. MIT CRISPR design (http://crispr.mit.edu) was used to design and predict the number of off-target events in the genome. When possible, the location of the gRNA-binding site was scattered along the chosen stretch of DNA and targeted to both the template (T) and non-template (NT) strands while

choosing the highest-ranking gRNAs with the least number of predicted off-target events in the genome.

The parental gRNA-expression vector (pgRNA-CKB) contained a "16nt" sequence (GGAGACGGACGTCTCC) with two BsmBI restriction sites for cloning the gRNA oligos. This vector served as the "scrambled" gRNA sequence. The gRNA-expression vector expressed only a single gRNA of interest from a mouse U6 promoter and contained a reporter and selection cassette with nuclear-localized mKate2-T2A-Blasticidin, driven off the CAG promoter. For cloning each gRNA into the expression vector (pgRNA-CKB), one forward oligo was designed with its reverse complement and ordered from Integrated DNA Technologies (IDT). In addition, a 4-nt overhang "TTGG" was added to the 5' end of the forward primer and a 4-nt overhang of "AAAC" was added to the 5' end of the reverse primer (see below for examples of gRNA oligos). Each forward and reverse oligo (100 µM) was placed in the same reaction, phosphorylated using T4 PNK (NEB), and annealed by first heating to 95ºC and then slowly ramping down to 25ºC at 5ºC per min. The pgRNA-CKB vector was digested with BsmBI (NEB), treated with FastAP (Life Technologies), and run on a 1% (w/v) agarose (Sigma) gel. The ~9.6 kb linear DNA fragment was extracted using the QIAquick Gel Extraction Kit (Qiagen). The linearized vector (50–100 ng) and diluted phospho-annealed oligos (1 µl of 1:100) were ligated overnight at room temperature with T4 DNA ligase (NEB). The ligated product was transformed into Turbo competent E. coli (NEB). Sequencing primers gRNA Seq F (5'-GAGATCCAGTTTGGTTAGTACCGGG-3') and gRNA Seq R (5'-ATGCATGGCGGTAATACGG TTAT-3') were used to confirm the ligation of the correct gRNA.

gRNA oligo sequences are listed as below. gRNA naming is based on the binding coordinates relative to the transcription start site (TSS) of the gene of interest, and whether they target the template (T) and non-template (NT) strand. A negative coordinate indicates a binding location upstream of the TSS and a positive coordinate indication a binding location downstream of the TSS. The most commonly used gRNAs for efficient knockdown are indicated with a bold text and column outline. Forward and reverse primers for cloning into the pgRNA-CKB gRNA-expression vector are listed from 5' to 3'. The 4-nt overhang sequences on the forward and reverse primers (highlighted in red) are used to clone phospho-annealed products into the pgRNA-CKB vector after BsmBI digest. The gRNA protospacer sequence is in black and designated as $(N)_{20}$ and the constant-tracer sequence is in blue.

5'–NNNNNNNNNNNNNNNNNNNNGTTTAAGAGCTATGCTGGAAACAGCATAGCAAGTTTAAATAAG
GCTAGTCCGTTATCAACTTGAAAAAGTGGCACCGAGTCGGTGCTTTTTTT –3'

gRNA Name (Targeting Strand)	Oligo Sequences 5' – Forward Primer – 3' 5' – Reverse Primer – 3'	Notes
OCT4 g–142 (T)	TTGGGGGGCGCCAGTTGTGTCTCC AAACGGAGACACAACTGGCGCCCC	

OCT4 g–105 (NT)	TTGGGGCGAAGGATGTTTGCCTAA AAACTTAGGCAAACATCCTTCGCC	
OCT4 g–7 (T)	TTGGAAGGCTAGTGGGTGGGACTG AAACCAGTCCCACCCACTAGCCTT	
OCT4 g–4 (T)	TTGGGCTAGTGGGTGGGACTGGGG AAACCCCCAGTCCCACCCACTAGC	Because the PAM-binding site contains an SNP at the *OCT4* locus, this gRNA binds to only one *OCT4* allele and knocks down *OCT4* by ~40%.
***OCT4* g+22 (NT)**	TTGGGGTGAAATGAGGGCTTGCGA AAACTCGCAAGCCCTCATTTCACC	*OCT4* g+22 is the most commonly used gRNA for efficient *OCT4* knockdown.
OCT4 g+42 (T)	TTGGTCGCAAGCCCTCATTTCACC AAACGGTGAAATGAGGGCTTGCGA	This gRNA does not knock down *OCT4*.
OCT4 g+56 (T)	TTGGTTCACCAGGCCCCCGGCTTG AAACCAAGCCGGGGGCCTGGTGAA	
OCT4 g+104 (NT)	TTGGACCACCTGGAGGGGGCGAGA AAACTCTCGCCCCCTCCAGGTGGT	This gRNA was used for both CRISPRi and CRISPRn
OCT4 g+126 (T)	TTGGTCGCCCCCTCCAGGTGGTGG AAACCCACCACCTGGAGGGGGCGA	This gRNA was used for both CRISPRi and CRISPRn
OCT4 g+701 (T)	TTGGCGAAGAGACAACTGCCGGTG AAACCACCGGCAGTTGTCTCTTCG	This gRNA does not knock down *OCT4*.
OCT4 g+1305 (NT)	TTGGGCTTACACTTGTCGCCTTGA AAACTCAAGGCGACAAGTGTAAGC	This gRNA does not knock down *OCT4*.
OCT4 g+2390 (NT)	TTGGGGAGTGCACTGGCGCGATCT AAACAGATCGCGCCAGTGCACTCC	This gRNA does not knock down *OCT4*.
OCT4 g+3410 (NT)	TTGGGTCTGTAAATCCTAGCACTT AAACAAGTGCTAGGATTTACAGAC	This gRNA does not knock down *OCT4*.
OCT4 g+4580 (T)	TTGGGTAGGTTCTTGAATCCCGAA AAACTTCGGGATTCAAGAACCTAC	This gRNA does not knock down *OCT4*.
OCT4 g+5632 (T)	TTGGCACCTCGCTTTCCCTAGCTC AAACGAGCTAGGGAAAGCGAGGTG	This gRNA does not knock down *OCT4*.
NANOG g–46 (T)	TTGGTCACAAGGGTGGGTCAGTAG AAACCTACTGACCCACCCTTGTGA	
NANOG g–29 (T)	TTGGTAGGGGGTGTGCCCGCCAGG AAACCCTGGCGGGCACACCCCCTA	
***NANOG* g+21 (NT)**	TTGGCCAGCAGAACGTTAAAATCC AAACGGATTTTAACGTTCTGCTGG	*NANOG* g+21 is the most commonly used gRNA for efficient *NANOG* knockdown.
NANOG g+38 (T)	TTGGCCAGGATTTTAACGTTCTGC AAACGCAGAACGTTAAAATCCTGG	
NANOG g+252 (NT)	TTGGCAGTCGGATGCTTCAAAGCA AAACTGCTTTGAAGCATCCGACTG	This gRNA was used for both CRISPRi and CRISPRn.
NANOG g+358 (T)	TTGGTTCTGCTGAGATGCCTCACA AAACTGTGAGGCATCTCAGCAGAA	This gRNA was used for both CRISPRi and CRISPRn.
SOX2 g–81 (T)	TTGGTCATGCAAAACCCGGCAGCG AAACCGCTGCCGGGTTTTGCATGA	
SOX2 g–56 (NT)	TTGGAGCGACCAATCAGCGCGCGG AAACCCGCGCGCTGATTGGTCGCT	
SOX2 g–44 (T)	TTGGAGGAGCCGCCGCGCGCTGAT AAACATCAGCGCGCGGCGGCTCCT	
SOX2 g–9 (NT)	TTGGGACAACCATCCATGTGACGG AAACCCGTCACATGGATGGTTGTC	
***SOX2* g–1 (T)**	TTGGCCCTGACAGCCCCCGTCACA AAACTGTGACGGGGGCTGTCAGGG	*SOX2* g–1 is the most commonly used gRNA for efficient *SOX2* knockdown.
BAG3 g–95 (NT)	TTGGTTCCGACTCGTGCGCGTGCC AAACGGCACGCGCACGAGTCGGAA	
BAG3 g–2 (NT)	TTGGGTCATCGGCTATAATCGCGG	

	AAACCCGCGATTATAGCCGATGAC	
BAG3 g+64 (T)	TTGGCGGGCCGCGGCCAACTTCTC AAACGAGAAGTTGGCCGCGGCCCG	
***BAG3* g+212 (T)**	TTGGTTCATAAAGGTGCCCGGCGC AAACGCGCCGGGCACCTTTATGAA	*BAG3* g+212 is the most commonly used gRNA for efficient *BAG3* knockdown.
***ROCK1* g+11 (NT)**	TTGGCGGGGCGCGGACGCTCGGAA AAACTTCCGAGCGTCCGCGCCCCG	*ROCK1* g+11 is the most commonly used gRNA for efficient *ROCK1* knockdown.
ROCK1 g+47 (NT)	TTGGCAAACAAACGGAGACCGCCG AAACCGGCGGTCTCCGTTTGTTTG	
ROCK1 g+119 (NT)	TTGGAGTCGCGGCGGCGAATGCCT AAACAGGCATTCGCCGCCGCGACT	
ROCK1 g+196 (NT)	TTGGAGACGATAGTTGGGTCCCGG AAACCCGGGACCCAACTATCGTCT	
GSK3β g–97 (NT)	TTGGGGATCCGGCGGGCTGACGGC AAACGCCGTCAGCCCGCCGGATCC	
GSK3β g–82 (NT)	TTGGCTCCGGCAAGCCGCGGGATC AAACGATCCCGCGGCTTGCCGGAG	
GSK3β g–67 (T)	TTGGCGCCGGATCCCGCGGCTTGC AAACGCAAGCCGCGGGATCCGGCG	
***GSK3β* g–48 (NT)**	TTGGGGGTGGCTCGGAGATGCGAC AAACGTCGCATCTCCGAGCCACCC	*GSK3β* g–48 is the most commonly used gRNA for efficient *GSK3β* knockdown.
***HERG* g–175 (T)**	TTGGTTCTGGGCGCGCGAGTCCCA AAACTGGGACTCGCGCGCCCAGAA	*HERG* g–175 is the most commonly used gRNA for efficient *HERG* knockdown in iPSC and iPS-CM.
HERG g–127 (T)	TTGGCGTTGGGGGAGCACTCGGCG AAACCGCCGAGTGCTCCCCCAACG	
HERG g–11 (NT)	TTGGTAATGCGGCGCGCGCCCCTC AAACGAGGGGCGCGCGCCGCATTA	
HERG g+22 (T)	TTGGCGCATTAACCCTTCCGCGGC AAACGCCGCGGAAGGGTTAATGCG	
MESP1 g–124 (T)	TTGGTGGGTCGGGCGCCCAAGCGA AAACTCGCTTGGGCGCCCGACCCA	
MESP1 g–56 (T)	TTGGCCCCCCGCCGTGGATTCAAA AAACTTTGAATCCACGGCGGGGGG	
***MESP1* g+22 (NT)**	TTGGGCCGCTTTATGCCGAGCCCG AAACCGGGCTCGGCATAAAGCGGC	*MESP1* g+22 is the most commonly used gRNA for efficient *MESP1* knockdown.
MESP1 g+45 (T)	TTGGGCTCGGCATAAAGCGGCCGC AAACGCGGCCGCTTTATGCCGAGC	
MYBPC3 g–174 (T)	TTGGAATTGTGCTGCGGGGGGTGA AAACTCACCCCCCGCAGCACAATT	
MYBPC3 g–21 (T)	TTGGGGGAGGTCCCCATATATAGT AAACACTATATATGGGGACCTCCC	
***MYBPC3* g+26 (NT)**	TTGGCGTCACACCAGGCACGAAGC AAACGCTTCGTGCCTGGTGTGACG	*MYBPC3* g+26 is the most commonly used gRNA for efficient *MYBPC3* knockdown.
MYBPC3 g+36 (T)	TTGGACCTGTGCCTGCTTCGTGCC AAACGGCACGAAGCAGGCACAGGT	
MYBPC3 g+52 (T)	TTGGTGCCTGGTGTGACGTCTCTC AAACGAGAGACGTCACACCAGGCA	
GCaMP g+24 (T)	TTGGTTGACTCATCACGTCGTAAG AAACCTTACGACGTGATGAGTCAA	gRNAs target the template strand of GCaMP6f open reading frame. Unlike guides targeting endogenous loci, the coordinates of the GCaMP guides are based on the translation start site (starting
***GCaMP* g+56 (T)**	TTGGGGTCACGCAGTCAGAGCTAT AAACATAGCTCTGACTGCGTGACC	

GCaMP g+91 (T)	TTGGACTCGAGAACGTCTATATCA AAACTGATATAGACGTTCTCGAGT	from ATG). GCaMP g+56 was the most efficient guide at knockdown and was used for the reversibility and RNA-Seq experiments.
CD4 g+16 (NT)	TTGGGCTCCTCCACACCCTAGGCC GTTTAAGAGC TTAGCTCTTAAACGGCCTAGGGTG TGGAGGAGCCCAACAAG	gRNA oligo sequences targeting near the *CD4* TSS targeting either the template (T) or non-template (NT) strand. *CD4* gRNA oligos were annealed and cloned into the pSLQ1371 lentiviral expression vector using BstXI and BlpI (Gilbert et al., 2014). CD4 g+187 (NT) was the most efficient gRNA at *CD4* knockdown.
CD4 g+187 (NT)	TTGGAGTCTGACCACCTTACCTCT GTTTAAGAGC TTAGCTCTTAAACAGAGGTAAGGT GGTCAGACTCCAACAAG	
CD4 g+189 (T)	TTGGCAAGAAAGACGCAAGCCCAG GTTTAAGAGC TTAGCTCTTAAACCTGGGCTTGCG TCTTTCTTGCCAACAAG	

Genomic DNA Preparation from Cells

Genomic DNA was extracted from ~10^5 cells with the DNeasy Blood & Tissue Kit (Qiagen). DNA samples were eluted in dH_2O, and sample concentrations were normalized to 100 ng/µl.

Genotyping Junction PCR

100 ng of genomic DNA were used in a 25 µl of PCR reaction mix using Phusion High-Fidelity DNA Polymerase (NEB). Standard PCR conditions were used: 62ºC annealing temperature and 30 seconds of extension at 72ºC per 1 kb of product. Primers used for genotyping PCR amplification are listed below.

Genotyping PCR Primers

Primer	Primer sequence (5' – 3')	Notes
WT AAV F	CGGTTAATGTGGCTCTGGTT	Amplifies the WT AAVS1 junction spanning the TALEN cut site. Expected PCR product size = 254 bp
WT AAV R	AGGATCCTCTCTGGCTCCAT	
AAV 5'J F	CTGCCGTCTCTCTCCTGAGT	Amplifies the 5' integration junction of knock-in vectors into the AAVS1 locus Depending on the antibiotic resistance of the knock-in vector either the Neo J R or the Puro J R primer should be used For Puro junction: Expected PCR product size = 1068 bp For Neo junction: Expected PCR product size = 1258 bp
Neo J R	CTCGTCCTGCAGTTCATTCA	
Puro J R	GTGGGCTTGTACTCGGTCAT	

TOPO TA Cloning and Sequencing

Genomic DNA was extracted from CRISPRi and CRISPRn clones containing *OCT4* and *NANOG* gRNA before and after doxycycline treatment. The region spanning the first exon of *OCT4* and *NANOG* was amplified using amplification primers listed below using Phusion High-Fidelity DNA Polymerase (NEB). PCR products were cloned into TOPO-TA cloning vector (Life Technologies) and transformed into Turbo competent *E. coli* (NEB) according to manufacturer's instructions. For each condition, individual colonies (13–48) were picked and plasmid DNA was isolated using the QIAprep Spin Miniprep Kit (Qiagen) and sequenced using the T7 primer.

***OCT4* and *NANOG* Amplification Primers**

Primer	Primer sequence (5' – 3')	Notes
OCT4 Seq F	TCCACCCATCCAGGGGGCGG	For genomic DNA amplification around the first exon of *OCT4* to identify mutations Expected PCR product size = 580 bp
OCT4 Seq R	CATGACCACCTCCCCACACC	
NANOG Seq F	CTTTTCCTTCTGGAGGTCCTAT	For genomic DNA amplification around the first exon of *NANOG* to identify mutations Expected PCR product size = 400 bp
NANOG Seq R	GGATTAGTTGATAATAACACTTCTTTA	

Copy Number Assay using Droplet Digital PCR

50 ng of genomic DNA from each sample was digested with 2.5 U of HaeIII (NEB) in 1x CutSmart buffer in a total volume of 20 µl. Samples were incubated at 37ºC for 1 h and then heat inactivated at 65ºC for 20 min. 5 µM of each forward and reverse primer and 18 µM Taqman MGB (FAM) probe for Neomycin or Puromycin-resistance genes (kindly provided by Jen Berman and Samantha Cooper at Bio-Rad) were mixed in dH_2O. ddPCR reactions took place in a total volume of 25 µl containing 2 µl of digested DNA, 12.5 µl of 2x ddPCR Supermix for Probes (Bio-Rad), 1.25 µl of the premixed (FAM) primers/probe mixture, 1.25 µl of 20X (HEX) RPP30 reference primers/probe premix (Bio-Rad) and 10 µl dH_2O. Droplet generation was performed according to the manufacturer's instructions on a QX100 Droplet Generator (Bio-Rad). The ddPCR thermocycling conditions were: step 1, 95ºC 10 min; step 2, 94ºC 30 s; step 3, 58ºC (pre-optimized) 1 min; repeat steps 2 and 3 39 times; step 4, 98ºC 10 min. The PCR amplified droplets were analyzed on the QX100 droplet reader (Bio-Rad) with the chosen setting "CNV2" (for 2 copies). The copy number was analyzed using Quantasoft software (Bio-Rad).

Primers and Probes for ddPCR Assay

Primer / Probe	Primer / Probe sequence (5' – 3')	Notes
ddPCR-NeoF Primer	CATGGCTGATGCAATGCG	Optimal annealing temp = 58ºC Expected Amplicon size = 68 bp
ddPCR-NeoR Primer	TCGCTTGGTGGTCGAATG	

ddPCR-Neo Probe	CGCTTGATCCGGCTACCTGCC	
ddPCR-PuroF Primer	GTCACCGAGCTGCAAGAA	Optimal annealing temp = 58ºC Expected Amplicon size = 57 bp
ddPCR-PuroR Primer	CACCTTGCCGATGTCGAG	
ddPCR-Puro Probe	CTCTTCCTCACGCGCGTCGG	

Karyotyping
Samples were sent to Cell Line Genetics for karyotypic analyses, where 20 metaphases were analyzed using G-band karyotyping.

Immunocytochemistry
Cells were fixed in 4% (v/v) paraformaldehyde (Affymetrix) in PBS for 15 min and permeabilized in 0.1% (v/v) Triton X-100 (Sigma) for 15 min. Cells were blocked in 5% (w/v) bovine serum albumin (BSA) (Sigma) with 0.1% (v/v) Triton X-100 in PBS for 60 min. Cells were incubated overnight at 4ºC with primary antibodies diluted in 5% (w/v) BSA and 0.1% (v/v) Triton X-100 in PBS. Then, cells were washed three times in PBS for 15 min each. Cells were then incubated for 1 h at room temperature with secondary antibodies diluted in 5% (w/v) BSA and 0.1% (v/v) Triton X-100 in PBS. Then, cells were washed three times in PBS for 15 min each. Finally, cell nuclei were counterstained using VECTASHIELD mounting medium with DAPI (Vector Laboratories). Images were taken under a Zeiss Axio Observer microscope and processed using ZEN 2012 software version 8.0. Table below contains a list of the primary and secondary antibodies and their appropriate dilution.

Flow Cytometry
iPSCs and iPS-CMs were singularized with accutase. Cells were washed twice with PBS and fixed in 4% (v/v) paraformaldehyde (Affymetrix) in PBS for 10 min. Cells were then pelleted and washed with chilled (4ºC) FACS buffer consisting of 0.5% BSA (w/v) and 2 mM EDTA in PBS. Next, the samples were incubated in primary antibody for 30 min, followed by three washes in PBS. Finally, the samples were incubated in the appropriate secondary antibody for 30 min, followed by washes in PBS. Table below lists the antibodies used for these experiments. All experiments that measure GCaMP or mCherry intensity were performed on live cells without fixation, immediately after harvesting in PBS. For each sample, 20,000 events were captured on the MACSQuant VYB flow cytometer and analysed with FlowJo X 10.0.7r2.

Western blots
Cell pellets were collected, washed with PBS and resuspended in RIPA lysis buffer (150 mM NaCl, 1 mM EDTA, 0.5% sodium deoxycholate, 50 mM Tris-HCl, 0.1% SDS, 2% TritonX-100, pH 8.0) containing a protease inhibitor cocktail (Roche). Samples were incubated for 30 min on ice and sonicated for 10 sec. 20 µg of each lysate were loaded per lane of a NuPAGE 4–12% Bis-Tris

polyacrylamide gel (Life Technologies). The gel was transferred onto a Nitrocellulose iBlot gel transfer stack using the iBlot gel transfer device (Life Technologies). The membrane was blocked in Odyssey Blocking Buffer (PBS) (LI-COR) for 1 h. Membranes were probed with the appropriate primary and secondary antibodies listed in the Table below. All primary antibodies were incubated overnight at 4ºC while secondary antibodies were left at room temperature for 1 h. Blots were imaged using the Odyssey Fc imaging system (LI-COR). Quantification of band intensities was performed using imageJ.

Primary and Secondary Antibodies

Type	Antibody	Application	Dilution	Species	Manufacturer and Catalog Number
Primary	Anti-OCT4	Immunocytochemistry	1:200	Mouse monoclonal	Santa Cruz Biotechnology sc-5279
		Western blot	1:1000		
		Flow cytometry	1:50		
	Anti-NANOG	Immunocytochemistry	1:200	Mouse monoclonal	Millipore MABD24
		Western blot	1:1000		
	Anti-SOX2	Immunocytochemistry	1:200	Rabbit polyclonal	Abcam ab59776
	Anti-BAG3	Immunocytochemistry	1:2000	Rabbit polyclonal	Abcam ab47124
	Anti-MYBPC3	Immunocytochemistry	1:200	Rabbit polyclonal	Abcam ab110832
		Western blot	1:1000		
	Anti-ACTN2	Immunocytochemistry	1:500	Mouse monoclonal	Sigma A7732
		Western blot	1:1000		
	Anti-TNNT2	Flow cytometry	1:100	Mouse monoclonal	Thermo scientific MS-295-P1
	Anti-GAPDH	Western blot	1:1000	Rabbit polyclonal	Abcam ab9485
	Anti-FLAG	Flow cytometry	1:100	Mouse monoclonal	Sigma F3165
	Anti-Cas9	Immunocytochemistry	1:200	Mouse monoclonal	Diagenode C15200203
		Western blot	1:1000		
		Flow cytometry	1:100		
	Anti-CD4 APC-Conjugated	Flow cytometry	1:100	Mouse monoclonal	BD 555349
Secondary	Goat anti-Mouse IgG (H+L), Alexa Fluor 647 conjugate	Immunocytochemistry	1:500	Goat anti-mouse IgG (H+L)	Life Technologies A-21236
	Chicken anti-Rabbit IgG (H+L), Alexa Fluor 647 conjugate	Immunocytochemistry	1:500	Chicken anti-rabbit IgG (H+L)	Life Technologies A-21443

	Goat anti-Mouse IgG (H+L), Alexa Fluor 488 conjugate	Immunocytochemistry	1:500	Goat anti-mouse IgG (H+L)	Life Technologies A-11001
	IRDye® 800CW Donkey anti-Rabbit IgG (H + L)	Western blot	1:2500	Donkey anti-rabbit IgG (H + L)	Li-COR 926-32213
	IRDye® 680LT Donkey anti-Mouse IgG (H + L)	Western blot	1:2500	Donkey anti-mouse IgG (H + L)	Li-COR 926-68022

CRISPRi and CRISPRn Knockdown and Knockout Assays in iPSCs

Initial rounds of knockdown or knockout screening with different gRNAs per gene were performed in polyclonal populations (greater than ~90% positive for mKate2). Unless specified, in all knockdown and knockout assays, iPSCs were cultured in mTeSR supplemented with doxycycline (2 μM; Sigma) for 7 continuous days before analysis. All corresponding negative controls (minus doxycycline) were maintained in mTeSR for 7 days. After identifying the most efficient gRNAs by TaqMan qPCR, immunocytochemistry, or flow cytometry, polyclonal populations of cells carrying the most efficient gRNA were subcloned by serial dilution. Subsequent analysis and assays were performed on clonal populations to obtain clean knockdowns or knockouts.

CRISPRi Knockdown Assays in Cardiac Mesoderm and iPS-CM

For CRISPRi knockdown in cardiac progenitor cells, stable iPSCs containing gRNA were differentiated towards the cardiac lineage with the WNT-differentiation protocol (described below). Half of the samples were treated with doxycycline (2 μM) from day 0 of differentiation (Figure S5A). Samples were harvested on day 4 of differentiation and analyzed using Taqman qPCR. For CRISPRi knockdown in iPS-CM, stable polyclonal iPSCs containing gRNA were differentiated into iPS-CM. On day 5 of differentiation, cells were enzymatically dissociated and replated onto Matrigel-coated plates at a density of $2.5x10^4$ cells/cm^2. Half of the cells were treated with media supplemented with doxycycline (2 μM) and the other half was treated with media only. Doxycycline was maintained throughout the differentiation process (either day 15 for non-lactate-treated cells or day-35 for lactate-treated cells) until cells were harvested.

RNA Extraction and TaqMan qPCR Analysis

RNA was extracted from approximately 10^5 cells with TRIzol reagent (Life Technologies) and cleaned up with the PureLink RNA Kit (Life Technologies) according to manufacturer's instructions. Samples were then treated with DNaseI (Life Technologies) for 30 min at 37ºC. Then, 1 μg of total RNA was reverse-transcribed into first-strand cDNA using SuperScript III (Life Technologies) with random hexamers, following the manufacturer's instructions. Real-Time qPCR reactions were performed in TaqMan Universal PCR Master Mix (Life Technologies) with the TaqMan probes listed in the table below. Quantification of gene expression was carried out with probes against the target gene and normalized against three ubiquitously expressed endogenous controls *18S*,

GAPDH, and *UBC* for iPSCs and cardiac mesoderm cells. For iPS-CM, qPCR results were validated with three independent biological replicates to minimize batch-to-batch variability in the timing of cardiac-specific marker expression. In addition to three housekeeping genes (18S, *GAPDH*, and *UBC*), two cardiac-specific markers (*TNNT2* and *MYH6*) were used to normalize expression of target genes. Relative expression of the gene of interest was normalized against endogenous or cardiac-specific genes using the difference in threshold-cycle (C_T) values between the gene of interest and endogenous control by the $2^{-\Delta\Delta C}{}_T$ method (Schmittgen and Livak, 2008).

TaqMan qPCR Probes

Gene Probe	Gene ID	Exon Boundary	Amplicon Length (bp)	Marker
OCT4	Hs00742896_s1	1–1	65	Pluripotency
NANOG	Hs02387400_g1	1–2	109	Pluripotency
SOX2	Hs01053049_s1	1–1	91	Pluripotency
ROCK1	Hs01127699_m1	1–2	79	Kinase
GSK3β	Hs01047719_m1	1–2	65	Kinase
BAG3	Hs00188713_m1	1–2	83	Co-chaperone protein
HERG	Hs00542479_g1	6–7	67	K^+ Ion channel
PAX6	Hs01088112_m1	4–5	55	Neuronal marker
T	Hs00610080_m1	8–9	132	Mesoderm marker
MESP1	Hs00251489_m1	1–2	80	Cardiac mesoderm marker
MYBPC3	Hs00165232_m1	12–13	56	Cardiac sarcomeric protein
TNNT2	Hs00165960_m1	10–11	89	Cardiac sarcomeric protein
MYH6	Hs01101425_m1	20–21	67	Cardiac sarcomeric protein
UBC	Hs00824723_m1	1–2	71	Housekeeping
18S	Hs99999901_s1	1–1	187	Housekeeping
GAPDH	Hs02758991_g1	6–7	93	Housekeeping

iPS-CM Differentiation

iPSCs were differentiated into iPS-CM using the WNT modulation-differentiation method (Lian et al., 2012) (Figure S5A). Briefly, iPSCs were seeded at 1.25–2.5x10^4 cells/cm^2 onto cell-culture plates coated with 80 μg/μl growth factor-reduced Matrigel (BD Biosciences) in mTeSR supplemented with 10 μM Y-27632 (Selleckchem) for 24 h (day –3). mTeSR medium was changed daily for the next 2 days. On day 0, iPSCs were treated with 12 μM CHIR99021 (CHIR) (Tocris) in RPMI/B27 without insulin (Life Technologies) for exactly 24 h. On day 1, the culture medium was replaced with fresh RPMI/B27 without insulin and maintained for 48 h. On day 3, cells were treated with 5 μM IWP2 (Tocris) in RPMI/B27 without insulin and maintained for 48 h. On day 5, fresh RPMI/B27 without insulin was added to the cells, and on day 7, the medium was switched to RPMI/B27 with insulin. Afterward, fresh RPMI/B27 with insulin was added to the

cells every 3 days. Functional iPS-CM appeared in culture between days 8 and 10 post-CHIR treatment.

Lactate Purification of iPS-CM

iPS-CM were purified via a modified version of the lactate metabolic-selection method (Tohyama et al., 2013). Briefly, 1 M lactate-stock solution was prepared in 1 M HEPES buffer (Sigma) with sodium L-lactate powder (Sigma). Glucose-free DMEM (Life Technologies) supplemented with 4 mM lactate solution, 1X Glutamax, and 1X non-essential amino acids (Life Technologies) was prepared as the selection medium. On day 15 post-CHIR treatment, iPS-CMs were split 1:2 onto Matrigel-coated 10-cm dishes in RPMI/B27 (Life Technologies) supplemented with insulin and Y-27632 (10 μM). Replated cells were allowed to recover for 5 days in RPMI/B27 supplemented with insulin before selection. Cells were then washed with PBS and incubated in lactate-selection medium, changed every other day for 4 days. Then, the medium was replaced with RPMI/B27 supplemented with insulin. Cells were allowed to recover for 3 days before being harvested.

Calcium-Transient Analysis of iPS-CMs

Lactate-purified iPS-CMs were replated onto Matrigel-coated plates and allowed to recover for 10 days before phenotypic analysis and immunostaining. Calcium transients in iPS-CMs were measured using the GCaMP signal to indicate intensity changes in GFP-flourescence. Videos were recorded with a Zeiss Axio Observer microscope, processed with ZEN 2012 software version 8.0, and analyzed with ImageJ.

Electrophysiology

Contracting iPS-CM were dissociated with trypsin (0.25%) and replated onto Matrigel-coated coverslips. After reconfirming visible beating, coverslips were placed in a superfusion bath (Warner, RC26-GLP) on a Nikon TiS inverted microscope equipped with a microfluorometer (IonOptix LLC). Superfusion solutions were warmed to 30°C with a superfusion system and heated perfusion pencil (ValveLink, AutoMate Scientific). Small clusters (five or fewer cells) of spontaneously contracting iPS-CMs were selected for study, with one cell under amphotericin B-perforated patch clamp (Spencer et al., 2014). Briefly, patch electrodes of approximately 2–4 MΩ (WPI) were tip-filled by dipping (20 s) them in an intracellular solution containing: KCl (120 mM), NaHEPES (20 mM), MgATP (10 mN), K_2EGTA (5 mM), $MgCl_2$ (2 mM), and adjusted to pH 7.1 with KOH. This solution was then back filled with the same solution, including amphotericin B (240 μg/ml). Coverslips were superfused at a constant flow (Warner, DN series) with modified Tyrode's extracellular solution containing: NaCl (137 mM), NaHEPES (10 mM), dextrose (10 mM), KCl (5 mM), $CaCl_2$ (2 mM), and $MgCl_2$ (1 mM), set to pH 7.4 with NaOH. Spontaneous action potentials (APs) were recorded in current clamp mode with zero applied current, and Ca^{2+} signals were low-pass filtered at 2 kHz and digitized at 5 kHz for 30 s per data file.

Supplemental References

Gilbert, L.A., Horlbeck, M.A., Adamson, B., Villalta, J.E., Chen, Y., Whitehead, E.H., Guimaraes, C., Panning, B., Ploegh, H.L., Bassik, M.C., et al. (2014). Genome-Scale CRISPR-Mediated Control of Gene Repression and Activation. Cell *159*, 647–661.

Lian, X., Hsiao, C., Wilson, G., Zhu, K., Hazeltine, L.B., Azarin, S.M., Raval, K.K., Zhang, J., Kamp, T.J., and Palecek, S.P. (2012). Robust cardiomyocyte differentiation from human pluripotent stem cells via temporal modulation of canonical Wnt signaling. Proc. Natl. Acad. Sci. 201200250.

Okita, K., Matsumura, Y., Sato, Y., Okada, A., Morizane, A., Okamoto, S., Hong, H., Nakagawa, M., Tanabe, K., Tezuka, K., et al. (2011). A more efficient method to generate integration-free human iPS cells. Nat. Methods *8*, 409–412.

Schmittgen, T.D., and Livak, K.J. (2008). Analyzing real-time PCR data by the comparative CT method. Nat. Protoc. *3*, 1101–1108.

Spencer, C.I., Baba, S., Nakamura, K., Hua, E.A., Sears, M.A.F., Fu, C., Zhang, J., Balijepalli, S., Tomoda, K., Hayashi, Y., et al. (2014). Calcium Transients Closely Reflect Prolonged Action Potentials in iPSC Models of Inherited Cardiac Arrhythmia. Stem Cell Rep. *3*, 269–281.

Tohyama, S., Hattori, F., Sano, M., Hishiki, T., Nagahata, Y., Matsuura, T., Hashimoto, H., Suzuki, T., Yamashita, H., Satoh, Y., et al. (2013). Distinct Metabolic Flow Enables Large-Scale Purification of Mouse and Human Pluripotent Stem Cell-Derived Cardiomyocytes. Cell Stem Cell *12*, 127–137.